ANALYSIS OF THE ELECTRON SPIN RESONANCE SPECTRUM OF A PREFERENTIALLY ORIENTED DEFECT CENTER IN DIAMONDS

By

WILLIAM CARL STECKELBERG

Bachelor of Science

Carnegie Institute of Technology

Pittsburg, Pennsylvania

1964

Submitted to the faculty of the Graduate College
of the Oklahoma State University
in partial fulfillment of the requirements
for the Degree of
DOCTOR OF PHILOSOPHY
May, 1971

ANALYSIS OF THE ELECTRON SPIN RESONANCE SPECTRUM OF A PREFERENTIALLY ORIENTED DEFECT CENTER IN DIAMONDS

Thesis Approved:

William J. Lowe
Thesis Adviser

Leon W. Schroeder

Harold Bristow

A. D. Buchan
Dean of the Graduate College

ACKNOWLEDGMENTS

The author would like to express his sincere gratitude to Dr. W. J. Leivo for his help, guidance, and constant encouragement during the course of this investigation.

The cooperative atmosphere among those associated with the research in diamond is deeply appreciated. Particular thanks are extended to P. Klingsporn who assisted in the taking of the data and for his continued interest in the research. Thanks are also extended to Dr. M. D. Bell for his interest and interesting discussions on the study.

The diamonds used in the study were kindly made available by Dr. J. F. H. Custers, Research Consultant, Industrial Distributers (1946) Limited, South Africa, and Dr. H. B. Dyer, Director, Diamond Research Laboratory, South Africa. The author would like to thank Dr. Custers and Dr. Dyer for their continued interest and assistance in the diamond research at Oklahoma State University.

Financial support administered through the Research Foundation and made available by the National Science Foundation is gratefully acknowledged.

TABLE OF CONTENTS

LIST OF TABLES

LIST OF FIGURES

LIST OF FIGURES (Continued)

CHAPTER I

INTRODUCTION

Preliminary Remarks

Electron paramagnetism occurs when a resultant angular momentum due to the presence of an unpaired electron exists. Electron paramagnetic resonance[1] is produced when the unpaired electron interacts with an applied alternating magnetic field producing transitions between Zeeman levels, which are produced by an externally applied static magnetic field. The first successful electron spin resonance measurements were made by Zavoisky (1).

There are several classes of materials which give rise to electron paramagnetism. Atoms and molecules which have an odd number of electrons or molecules with a resultant angular momentum, transition elements with unpaired electron spins in an inner shell, semiconductors with electron donor levels, metals and semiconductors having electrons in the conduction band, free radicals, color centers or any crystal defect with an associated electron will all exhibit electron paramagnetism.

The major effort of this research will be directed toward studies of diamond crystals which contain paramagnetic centers. The investigation of the ground state levels of paramagnetic centers which are con-

---

[1] Electron paramagnetic resonance or electron spin resonance will be abbreviated as ESR when appropriate.

tained in single crystals as impurities or inclusions, and the effects upon the energy levels of the ion caused by the internal crystalline fields have been very fruitfully investigated through ESR techniques. The contribution to the susceptibility of a very dilute concentration of paramagnetic centers in a crystal can be singled out and investigated using ESR techniques.

A perfect natural diamond would have the properties of an insulator; in fact, the band gap has been shown to be on the order 5.5 eV; however, in 1952 J. F. H. Custers found a diamond that conducted electricity. The electrical conductivity was shown to typify that of impurity activated semiconductors (2). However, an exact understanding of what impurities and in what manner the impurities are incorporated into the diamond crystals is still far from complete.

Since natural diamonds obviously depend on the environments in which they were formed, there will be unknown impurities and imperfections in different concentrations. It is, therefore, hopeful that a combination of information from different types of analysis will lead to a better understanding of the nature of the most predominant impurity levels that are present in the different types of diamonds.

The present study involves the investigation of the orientation dependence of the electron spin resonance spectrum observed in several Type I diamonds in our collection. A theoretical model is proposed from which the behavior of the spectrum can be predicted.

The Resonance Condition

A description of the resonance condition of a single crystal containing a dilute concentration of paramagnetic ions will be considered.

The ions will essentially be considered as free, non-interacting paramagnetic centers. In other words, the interaction of the electron associated with the paramagnetic center with the externally applied fields will be considered; the interaction with its surrounding environment will be neglected. Relaxation, spin-orbit interactions, spin-spin interactions, quadrupole interactions, hyperfine interactions and crystalline field effects will be considered in some detail later. The crystal is placed in a static magnetic field $\vec{H}_o$ which can be varied in strength and an alternating field $\vec{H}_1$, perpendicular to the static field. To obtain the resonance condition, the frequency of the alternating field is usually in the x-band of the microwave spectrum, and the static field strength is several thousand gauss. Also, the magntiude of the static field is usually much greater than the alternating field.

Associated with each of the unpaired electrons is a spin $\vec{S}$ in units of $\hbar$, where $\hbar$ is Plank's constant divided by 2π. An electron with spin $\vec{S}$ has a magnitude $|S| = \sqrt{s(s+1)}\,\hbar$ where s takes only the value $+\frac{1}{2}$. The spin $\vec{S}$ has a component in any direction given by S_z, where $S_z = m_s\hbar$, m_s ranging in value from -s to +s. Therefore, $m_s = \pm \frac{1}{2}$, or $S_z = \pm \frac{1}{2}\hbar$.

The fact that the magnitude of $\vec{S}$ and the z-component S_z of the spin angular momentum are related to the two quantum numbers s and m_s by

$$S = \sqrt{s(s+1)}\,\hbar ,$$

and

$$S_z = M_s\hbar$$

are identical to these for orbital angular momentum $L = \sqrt{\ell(\ell+1)}\,\hbar$ and $L_z = m_\ell\hbar$ where m_ℓ ranges from $-\ell$ to ℓ, should not lead one to think that spin has a classical analogue. In fact, both values of S_z vanish as $\hbar \to 0$ so that electron spin disappears as $\hbar \to 0$. In the case of

orbital angular momentum where $m_\ell = 0, \pm1, \pm2, \ldots$, a decrease of $\hbar$ in $m_\ell\hbar$ does not delimit the value of $m_\ell\hbar$. Therefore, no operator associated with S_z can be constructed from an operator associated with a classical dynamical variable.

There is also a magnetic moment $\vec{\mu}$ associated with each electron. The ratio of the magnetic moment to the spin is a constant γ, called the gyromagnetic ratio. The relationship between the spin and the magnetic moment is therefore given by

$$\vec{\mu} = -\gamma\hbar\vec{S}, \tag{1-1}$$

if the orbital contributions to the magnetic moment are neglected. This expression can also be written as

$$\vec{\mu} = -\frac{g\beta}{\hbar}\vec{S}$$

where β is the Bohr magneton and g is the spin factor and is usually referred to as the g-factor. In general, the g-factor is a 3 x 3 symmetric tensor of second rank. Therefore, a principal axis system will exist and will be denoted by g_1, g_2, g_3. In the case of a "free" ion with a resultant angular momentum J placed in a magnetic field,

$$g = 1 + \frac{J(J+1) + S(S+1) - L(L+1)}{2J(J+1)} \tag{1-2}$$

and is called the Landé g factor.

Initially the interaction of a single unpaired electron associated with a paramagnetic center will be considered. When the magnetic field is applied the Zeeman splitting arising from the spin degeneracy of the energy level will be produced. In the case of a single electron spin, two levels will be produced. The interaction energy between the static

field and the magnetic moment associated with the electron is $-\vec{\mu} \cdot \vec{H}_o$, where the static field in the z-direction is given by $\vec{H}_o = H_o \hat{k}$. The Hamiltonian for the spin system then can be written as

$$[H] = -\vec{\mu} \cdot \vec{H}_o \tag{1-3}$$

or

$$[H] = \gamma \hbar \vec{S} \cdot \vec{H}_o .$$

By substituting in the value for $\vec{H}_o$, the Hamiltonian becomes

$$[H] = \gamma \hbar H_o S_z . \tag{1-4}$$

Using the Dirac notation (3), the Schroedinger equation is

$$\gamma \hbar H_o S_z \mid \mu> = \gamma \hbar H_o m_s \mid \mu>,$$

where the eigenvalues m_s are $\pm \frac{1}{2}$. The energy levels of the electron are then given by $\pm \frac{1}{2} \gamma \hbar H_o$. The energy splitting of the two spin levels is given by

$$\Delta E = \gamma \hbar H_o = g \beta H_o \tag{1-5}$$

In general, the number of energy levels of an atom is $2S + 1$ where S is the total electron spin value, and the eigenvalues of S_z are

$$m_s = S, S-1, \ldots, -S.$$

A transition between the Zeeman levels can be induced by introducing an amount of energy ΔE given by Equation (1-5) into the spin system. Since $\Delta E = \hbar\omega$, where ω is the angular frequency of the radiation, then using Equation (1-5) the condition for a transition is given by

$$\hbar\omega = g \beta H \tag{1-6}$$

When a transition occurs, it is usually referred to as a "spin flip". This terminology arises from the classical consideration of the magnetic moment associated with the electron as being changed from a parallel to an anti-parallel orientation with respect to the magnetic field $\vec{H}_o$. It should be noted that for the case of multiple energy levels that the matrix element corresponding to each transition must be non-vanishing or the transition will be forbidden.

The g-factor of a paramagnetic ion in a crystal is defined experimentally by the equation

$$h\nu = g \beta H_o \tag{1-7}$$

where ν is the frequency of the radiation, or in this case the frequency of the applied alternating field $\vec{H}_1$. Equation (1-7) is usually referred to as the resonance condition. The g-factor is usually called the spectroscopic splitting factor and is not to be confused with the Landé g-factor given in Equation (1-2).

Diamond Studies

In a comprehensive study of diamond properties by Robertson, Fox, and Martin (4), diamonds were separated into two classes, denoted as Type I and Type II. The classifications are based primarily on the ultraviolet and infrared absorption characteristics of the diamonds. Type I diamonds have an increasing ultraviolet absorption characteristic for wave lengths shorter than approximately 3000 Å. They both have infrared absorption bands between 3μ and 6μ. The absorptive bands between 3μ and 6μ are probably due to the crystal lattice vibrational modes (5) and (6). The Type II crystal has an absorption edge in the ultraviolet region be-

low 2250 Å. The 2250 Å (5.5 eV) corresponds to the energy of the band gap between the valance and conduction bands, while the 3000 Å (4.15 eV) is due to impurity energy levels that are in the forbidden gap. These levels will be discussed in more detail later.

Some Type I diamonds are further separated into two sets corresponding to their infrared absorption lines (6). The absorption bands of the two groups always occur together and have the same relative intensity. The two groups are denoted as group A and group B. The characteristics of these groups are:

Group A

Infrared absorption bands: 7.8, 8.3, 1.1, and 20.8μ. The ultraviolet cut-off moves to a longer wavelength, and the 3155 Å intensity line increases with increasing infrared absorption.

Group B

Infrared absorption band: 7.0, 7.3, 7.5, 8.5, 10, 12.9, and 30.5μ. There is no correlation between these band intensities and the ultraviolet cut-off.

Type II diamonds have been divided into two classes (6) (7) (8). The first type is designated as Type IIb. It shows semiconductivity and phosphorescences in the far ultraviolet. Type IIa does not possess these properties. Type IIb diamonds are very rare.

Semiconducting diamonds are generally blue in color (9). This has been attributed to optical absorption in the red and infrared (10). Although the nature of the imperfections that produces this absorption is not completely understood, conductivity and a blue coloration have been

produced in synthetic diamonds by doping with boron (11). However, much experimental evidence indicates that semiconductivity is probably associated with aluminum acceptor states in natural diamonds.

Spectroscopic studies of Type I diamonds showed the most common non-gaseous impurities were generally Si, Ca, Mg, Al, Fe, Ti, and Cu in concentrations as large a 10^{18} impurity atoms per cc. (12). Type IIa and IIb both were found generally to contain the same amount of Si, Mg, and Al. However, similar non-gaseous impurities were found to be present in both types of diamonds and in similar concentrations.

Investigations to determine whether the difference in Type I and Type II diamonds could be attributed to carbon interstitials, carbon vacancies or clusters of vacancies instead of impurity atoms were pursued. However, subsequent work with diamonds irradiated with electrons, neutrons, and X-rays failed to produce infrared absorption bands in the 6μ to 13μ region (13). These investigations did give evidence of the formation of carbon interstitials and vacancies. Two systems of resonance lines were produced by neutron radiation and are given as follows:

(a) A single isotropic line with g-factor approximately 2.0. The intensity of this line decreases as the sample is heated to 1000°C.

(b) A less intense set of anisotropic lines which were not affected by heat. The symmetry of this set is parallel to any of the <110> axes[3]. These lines have been postulated to be due to carbon interstituals which form a more stable C_2 molecule and do not return to their

---

[3]A particular axis or direction in the crystal will be denoted by square brackets, such as [hkl]. A full set of equivalent directions in the crystal will be denoted by pointed brackets, such as <hkl>. For a particular set of planes in the crystal the notation will be a set of curved braces, such as (hkl), where the set of equivalent planes will be denoted by braces, such as {hkl}.

original positions upon heating (14). Observed broadening suggested that the vacancies were in clusters.

A study of the ESR spectra of diamonds irradiated with 2 MeV electrons again produced the single isotropic line, but the systems of anisotropic lines that were examined did not have the <110> symmetry axis observed by Griffiths et al (13) in the case of neutron irradiation (15). One system of up to 24 lines seemed to have a symmetry axis near the <221> direction and the second system of up to 6 lines had a <100> symmetry axis. Several theoretical models have been postulated concerning the nature of centers created by irradiation (16) (17) (18).

It was shown that in order to have sufficient coupling for single phonon absorption, the diamond lattice must contain impurities (19). The imperfections present in the Type I diamond producing the 7.8μ absorption band correspond to a single phonon absorption not present in Type II diamond (20).

The presence of anomalous X-ray spikes in the diffraction patterns of some diamonds led Frank (21) to hypothesize the existence of impurity platelets in the <100> planes. He assumed the impurities in the platelets to be silicon; however, the concentrations of silicon were found to be not nearly sufficient (22).

The differences in Type I and Type II diamonds were still not understood in 1959 when Kaiser and Bond (23) reported the discovery of concentration of nitrogen as high as 0.2% in Type I diamonds. The nitrogen was assumed to be present in substitutional lattice positions. The infrared absorption bands intensities were shown to be linearly proportional to the nitrogen concentration. In fact all the group A infrared absorption bands were attributed to carbon-nitrogen band vibrational

modes. The nitrogen was reported to form deep lying states in the forbidden energy gap corresponding to the 3156 $\mathring{A}$ absorption band characteristic of group A diamonds. There was no observed correlation of group B characteristics and the nitrogen concentration. Lightowler and Dean (24) repeated this study two years later and substantiated Kaiser and Bond's measurements. However, they did report that no correlation between the group B absorption and the 4150 $\mathring{A}$ ultraviolet absorption band seemed to exist.

The same year that Kaiser and Bond reported the detection of nitrogen in Type I diamonds, Smith, et al., (25) published a very important ESR study of nitrogen. The nitrogen was assumed to occupy a substitutional lattice position with the unpaired electron forming a hybridized sp^3 antibonding orbital along one of the carbon-nitrogen bonds. The electron was assumed to be localized on a single antibonding orbital with a degeneracy arising from the fact that it can be localized on any of the <111> bonding directions. Therefore, it would be expected that when $\vec{H}_o$ is parallel to one of the <100> directions, equal angles will be formed with the tetrahedral bonding producing the 2I + 1 hyperfine lines. The nitrogen atom has a nuclear spin I = 1 producing a hyperfine structure of three peaks with a ratios of 1:1:1.

The isotropic g-factor was found to be 2.0027 ± .0005. For an arbitrary orientation with respect to the <100> directions the side peaks split up into as many as four peaks.

The electron in the antibonding orbital is thought to be localized mainly about the carbon, not the nitrogen, atom (26). As a result of accommodating the unpaired electron in the σ-antibonding orbital the bond length between the nitrogen and carbon is increased approximately

11%. This also increases the p-character of the orbital.

The contribution of a small percent (1.1%) of C^{13} with spin I = ½ was also observed. However, when the concentration of nitrogen was calculated, it was found to be several orders of magnitude less than that measured by Kaiser and Bond. The number of spins was found to the 10^{15} to 10^{17} atoms per cc. It was assumed that the isolated donors comprised only a small percentage of the nitrogen present. The rest of the nitrogen was assumed to be present in a nonparamagnetic form such as adjacent substitutional pairs.

Elliott (27) speculated that nitrogen was the impurity atom that formed the platelets in the <100> planes. Evans and Phaal (28) confirmed the existence of impurity platelets in the <100> planes by using transmission electron microscopy. They also observed dislocation loops on the <111> planes in the same region with the impurity platelets. The loops were assumed to have resulted from the condensation of vacancies following the formation of the platelets. The presence of the denser concentration of nitrogen at the platelets further supports the possibility of the nitrogen being present in nonparamagnetic form. These two types of imperfections were not observed in Type II diamonds.

It is thought that the platelets of nitrogen in diamond are the cause of the anomalous X-ray reflections described as spikes passing through reciprocal lattice points parallel to <100> directions. James and Evans (29), using the dynamical theory of electron diffraction, computed profiles for the electron microscope images of impurity platelets found in the cube planes of Type I diamonds. They suggest the platelets contain a varying number of nitrogen-rich planes which produce a lattice displacement of approximately a/6, where a is the (400) interplanar

spacing. The diamond on either side of the platelets was observed to be compressed and some strain was detected in the plane of the platelets.

The diffraction spikes were appreciably decreased after heat treatment to 1160^{o} at 60 kilobars pressure for 14 minutes (30).

A recent study was made of broadened lines which coincide with normal, narrower nitrogen resonance lines (31). The broadening was assumed to be caused by dipole-dipole interaction of the unpaired spins associated with the nitrogen centers. It was assumed the existence of both the narrow and the broadened lines indicated the existence of regions of normal and enhanced concentrations respectively. Concentrations of 10^{20} atoms per cc were found to give rise to the broadened portion of the spectrum, while 3×10^{19} or less atoms per cc form the normal concentrations. This is in good agreement with nitrogen concentrations reported by Kaiser and Bond (23) and Lightowler and Dean (24).

The existence of additional weak lines with the nitrogen resonance have been classified into three groups (32). Group A lines were attributed to C^{13} in a second nearest neighbor position. Group B lines were shown to be interactions with the nitrogen quadrupole moment. Group C lines were found to be due to N^{15} with a nuclear spin $I = \frac{1}{2}$. The two lines of Group C were half way between the normal nitrogen resonance peaks with H_o//<100>.

The existence of aluminum as an acceptor state in diamonds has been postulated and studied using ESR (33). Aluminum having a nuclear spin $I = \frac{5}{2}$ should give rise to only 6 hyperfine lines. However, from 14-30 lines depending on the orientation with respect to $\vec{H}_o$ have been observed. The interaction of the quadrapole moment and the field gradient of the unpaired electron were assumed to permit forbidden transitions.

The symmetry axis of the ESR signed was found to be parallel to the <100> axes. Fourteen lines were observed in this direction. This spectrum is common in many diamonds.

In a study of the resonance signal of vacancies in diamond a Type IIa diamond with a very weak nitrogen resonance was irradiated with 0.75 MeV electrons (34). The isotropic line found by Griffiths et al (13) was found to be composed of three superimposed lines. The centers producing these lines were labeled A, B, and C. The energy used favored the formation of the A centers. The A center was found to have an anisotropic line width with the principal axis of the g-factor along the <100> directions. First and second nearest neighbor hyperfine interactions with C^{13} were detected. The hyperfine tensors were found to be uniaxial with principal axis along the <111> directions. The centers were ionized using light with energies of 2.83 eV and greater. The electrons produced were trapped in centers lying about 1.10 eV or more below the conduction band.

Electron spin resonance was detected in natural semiconducting diamonds (Type IIb) by Bell and Leivo (35). A similar resonance line was produced in Type Ia diamond as a result of crushing the diamond. There was also found to be a correlation between the ESR absorption and the magnitude of the p-type conductivity of the Type IIb diamonds investigated.

Klingsporn, Bell and Leivo reported an anisotropic ESR spectrum in Type Ib diamonds (36). It is characterized by a spin Hamiltonian of the form $H = \beta\vec{s}\cdot\vec{g}\cdot\vec{H} + \vec{A}\cdot\vec{I}\cdot\vec{S}$, where $S = \frac{1}{2}$ and $I = 1$, and where one of the components of the $\vec{A}$ and $\vec{g}$ tensor has a <110> orientation.

The effects of UV irradiation on the ESR spectrum of the sample used

in the majority of the experimental work in this study was done by King (37). The resonance which is the object of this study was found to be increased by irradiation at both 366 and 313 mμ. However, the substitutional nitrogen resonance was decreased in intensity by the UV irradiation.

In conclusion, an excellent review of selected topics in diamond research is contained in a text edited by R. Berman (38).

CHAPTER II

ELECTRON SPIN RESONANCE THEORY

Classical Theory

In considering electron spin resonance phenomenon the interaction of an electron spin system with an externally applied alternating magnetic field must be considered in more detail. The results derived will then be argued to hold for the total macroscopic magnetization of the sample. The consideration of this chapter will be primarily with reference to paramagnetic centers which are included in non-paramagnetic single crystals. A semiclassical theory of the frequency dependence of the complex susceptibility referred to as the Bloch equations (39) will be discussed. In the above discussions the interactions of the paramagnetic centers with their environment will be ignored. However, the effects of the crystalline field and subsequent orientation dependence will be briefly discussed in the last sections of this chapter.

Resonance and Rotating Coordinates

Consider the polarizing or static magnetic field to be in the z-direction and given by $\vec{H}_o = H_o\hat{k}$ in a stationary coordinate x, y, z, where $\hat{k}$ is the unit vector in the z-direction. If a magnetic moment $\vec{\mu}$ is associated with the electron, then the field will exert a torque on the electron given by $\vec{T} = \vec{\mu} \times \vec{H}_o$. As stated earlier, the magnetic moment associated with the electron is related to the spin angular momentum $\hbar \vec{S}$

by the equation $\vec{\mu} = -\gamma \hbar \vec{S}$. The equation of motion can then be obtained by noting that the time rate of change of angular momentum (which is equal to the torque) is given by

$$\hbar \frac{d \vec{S}}{d t} .$$

The equation of motion is then

$$\begin{aligned} \hbar \frac{d \vec{S}}{d t} &= \gamma \hbar \vec{S} \times \vec{H}_o, \text{ or} \\ \frac{d \vec{\mu}}{d t} &= \vec{\mu} \times \gamma \vec{H}_o . \end{aligned} \tag{2-1}$$

Since $\vec{\mu}$ in general cannot line up directly with the field $\vec{H}_o$, it will precess about $\vec{H}_o$ at a constant angle θ with respect to $\vec{H}_o$. The angular frequency at which $\vec{\mu}$ precesses about $\vec{H}$ is the Larmor frequency $\vec{\omega} = \gamma H_o \hat{k}$.

The most convenient method for solving equation (2-1) is to transform to a rotating coordinate system about the z-axes (40). Consider the rotating coordinate system x', y', z', where z' corresponds to the z-axis, as having an instantaneous angular velocity $\vec{\omega}$. The time rate of change of $\vec{\mu}$ in the rotating system is denoted by

$$(\frac{d\vec{\mu}}{dt})_{rot} , \text{ then}$$

$$\frac{d \vec{\mu}}{d t} = (\frac{d \vec{\mu}}{d t})_{rot} + \vec{\omega} \times \vec{\mu} . \tag{2-2}$$

Rearranging Equation (1-2) and combining with Equation (1-1) gives

$$\hbar (\frac{d \vec{\mu}}{a t})_{rot} = \gamma \hbar \vec{\mu} \times \vec{H}_{eff} , \tag{2-3}$$

where $\vec{H}_{eff} = \vec{H}_o - \vec{\omega}/\gamma$ is the effective field as observed in the rotating coordinate system. By choosing $\vec{\omega} = \gamma H_o \hat{k}$, then

$$\left(\frac{d\vec{\mu}}{dt}\right)_{rot} = 0 \quad \text{since} \quad \vec{H} = H_o \hat{k} .$$

Therefore, when $\omega_o = \gamma H_o$, where $\vec{\omega} = \vec{\omega}_o \hat{k}$, the magnetic moment $\vec{\mu}$ is a constant vector in the rotational coordinate system. This implies that the magnetic moment precesses about $\vec{H}_o$ or $\hat{k}$ with an angular frequency $\omega_o = \gamma H_o$, the Larmor frequency. By comparing this to Equation (1-6) it is seen that the precessional frequency is identical to the ESR absorption frequency.

As stated earlier, the application of the external magnetic field will remove the spin degeneracy of the electronic level. A transition or spin flip can be produced by the introduction of a quantum of radiation. Since the electron spin precesses about the field $\vec{H}_o$ at a constant velocity, then in order to make the spin flip to antiparallel direction with respect to $\vec{H}_o$, an alternating microwave field $\vec{H}_1$ must be applied in the plane perpendicular to the static field $\vec{H}_o$. The relative positions of the field and the spin are shown in Figure 1. When the sample resonance cavity is properly placed in the static field, it can be made to produce a plane polarized microwave field $\vec{H}_1$ perpendicular to $\vec{H}_o$. However, the plane wave can be considered as the sum of two circularly polarized components rotating in the opposite direction.

Consider the component of the field $\vec{H}_1$ which is rotating in the same sense as $\vec{\mu}$ as its frequency approaches the resonance condition given by Equation (1-6) (41). Arbitrarily assume the right-handed component of $\vec{H}_1$ is rotating in the same sense as $\vec{\mu}$ and is given by

$$\vec{H}_r = H_1 [\hat{i} \cos \omega_1 t + \hat{j} \cos \omega_1 t], \qquad (2\text{-}4)$$

where ω_1 is the microwave angular frequency and $\hat{i}$, $\hat{j}$, $\hat{k}$ are the unit vectors along x, y, z respectively. The field $\vec{H}_r$ applies a torque on $\vec{\mu}$ in the z-direction. Equation (1-1) can be written

$$\frac{d\vec{\mu}}{dt} = \vec{\mu} \times \gamma [\vec{H} + \vec{H}_r] \qquad (2\text{-}5)$$

Equation (2-5) can be transformed into the rotating coordinate system

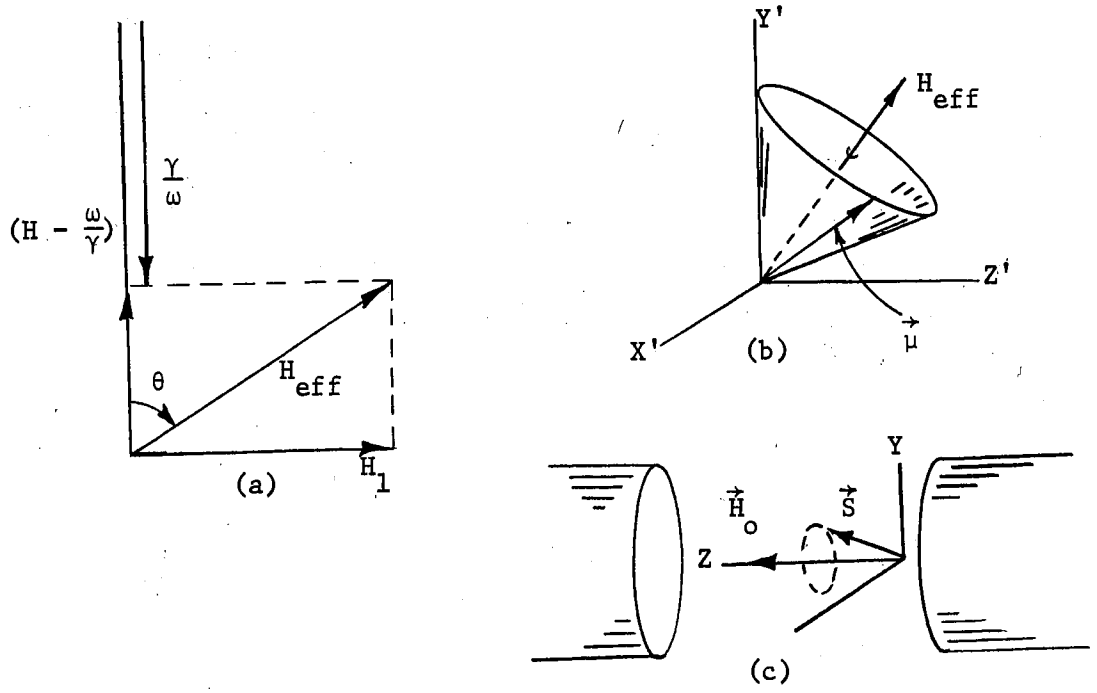

Figure 1. The Motion of the Magnetic Moment $\vec{\mu}$ in the Effective Magnetic Field $\vec{H}_{eff}$ and the Precession of $\vec{S}$ in the Magnetic Field H_o

with angular velocity $\vec{\omega} = \vec{\omega}_1 k$. The field component $\vec{H}_r$ will be a constant vector in the xy-plane and can be assumed to be arbitrarily directed along the x-axis as shown in Figure 1a. Then $\vec{H}_r$ is given by $\vec{H}_r = H_1 \hat{i}'$. Equation (2-5) in the rotating coordinate system is

$$\left(\frac{d\vec{\mu}}{dt}\right)_{rot} = \vec{\mu} \times \gamma \left[\left(H_o - \frac{\omega_1}{\gamma}\right) \hat{k}' + H_1 \hat{i}'\right]. \qquad (2\text{-}6)$$

In the rotating frame $\vec{\mu}$ precesses about the effective field

$$\vec{H}_{eff} = \left(H_o - \frac{\omega_1}{\gamma}\right) \hat{k}' = H_1 \hat{i}' \qquad (2\text{-}7)$$

as shown in Figure 1(b). From Equation (2-7), it can be seen that when the microwave frequency ω_1 is at the resonance condition the effective field is $\vec{H}_1 \hat{i}'$. The magnetic moment of the electron then precesses about H_1 with an angular frequency $\omega_p = \gamma H_1$. In general since $H_o >> H_1$, the frequency ω_p is much slower than ω_o. The magnetic moment of the electron in the rotating frame of reference is

$$\vec{\mu} = [\mu_x, \hat{k}' \cos \omega_p t - \mu_y, \hat{j}' \sin \omega_p t]. \qquad (2\text{-}8)$$

From Equation (2-8) it can be seen that the magnetic moment in the rotating frame periodically orients itself parallel and antiparallel to the static field $\vec{H}_o$ with a frequency ω_p. This corresponds to magnetic resonance phenomenon or spin flip at resonance. In the stationary frame the moment executes a helixical motion about the z-axis.

It should be noted that the magnetic vector component of $\vec{H}_1$ rotating in the opposite sense with respect to $\vec{\mu}$ applies no net torque on the magnetic moment. It should also be noted that no consideration was given to the electric field component of the microwave field. This is

because the spin flip is a magnetic dipole transition, and hence couples only with the magnetic component of the microwave field.

The interaction of independent electron spins with an alternating magnetic field has been discussed thus far. However, the total macroscopic magnetization is the quantity of interest. Equation (2-1) can be rewritten by considering the effect of all the dipoles per unit volume, such that the differential equation is simply written

$$\frac{d\vec{M}}{dt} = \gamma \vec{M} \times \vec{H} . \qquad (2\text{-}9)$$

Thus $\vec{M}$, the total magnetization per unit volume, rotates about the effective field $\vec{H}_{eff}$ at the Larmor frequency.

The Bloch Equations and Relaxation Effects

Relaxation

The description of the behavior of the macroscopic magnetization was developed by Bloch (39). The Bloch equations introduce the concept of relaxation times through a phenomenological description of the rate of change of magnetization of a paramagnetic material as an external magnetic field is applied. Their solution provides the frequency dependence of the complex susceptibility

$$\chi^* = \chi' - i\chi''. \qquad (2\text{-}10)$$

Bloch assumed that the systems of spins would tend exponentially toward thermal equilibrium. However, the specific mechanism by which the spins exchange energy with their surroundings does not enter into the phenomonological Bloch theory.

Spin Lattice Relaxation

There are basically two mechanisms by which the spins may exchange energy with their surroundings. The mechanisms are:

(1) spin-lattice relaxation, and

(2) spin-spin relaxation (42).

The Kronig (43) and Van Vleck (44) theories of the mechanism by which the spin system exchanges energy with the crystal lattice is in good agreement with low spin concentrations. The phonons of the lattice are coupled to the paramagnetic center charge distribution via the crystalline electric field. However, since the electron possesses no electric moment, the crystalline field must be coupled to the spin indirectly through the orbital angular momentum. The spin angular momentum and the orbital angular momentum are then in turn coupled through spin-orbit coupling. The spin lattice relaxation time can logically be seen to depend directly on the energy separation of the orbital levels and the strength of the spin-orbit coupling.

The spin may flip by either emitting or absorbing a single phonon of energy. This is usually predominant at low temperature and the associated relaxation time has a $1/T$ temperature dependence. For higher temperatures multiple scattering of higher energy phonons becomes predominant. The relaxation time associated with this process has a $1/T^7$ temperature dependence.

Spin-Spin Relaxation

A second relaxation process is spin-spin relaxation, which is more pronounced in crystals with high concentrations of paramagnetic centers. The internal field due to neighboring spin centers must be considered.

This field will be a fluctuating field with magnitude of the order of $H_i \approx \beta/r^3$, where r is the nearest neighbor distance. If the external field is much less than H_i, a reorientation of the effective field will be produced without a change in the magnitude. Hence, a net magnetization arises via an energy exchange between the spin system and the field. The spin will precess about H_i at the Larmor precession frequency γH_i, which gives rise to a spin-spin relaxation time $T_s \approx 1/\gamma H_i$. The spin-spin relaxation times are usually on the order of 10^{-10} second and are independent of temperature. A dispersion or spread of the precession frequency because of variations of the internal field at different nuclei is given by

$$\delta \omega_o \sim \frac{g \beta}{\hbar} H_i .$$

Two spins which have their spin relationships in phase at time t = 0 will have lost their phase relationship within time $1/\delta\omega_o$ second.

A second process that can interrupt the phases of the precessing spins is spin exchange. If two identical spin systems are antiparallel, the precessing component of the moment of one produces a precessing magnetic field at the other and vice versa. At the proper frequency the two spins could flip each other, leaving the net energy of the spin system unchanged. However, the process limits the lifetime of the spin state, and a spread in energy occurs according to the Heisenberg uncertainty relation. Both phase destroying processes impart to the absorption a finite line width.

The Bloch Equations

As stated earlier, Bloch introduced the concept of relaxation times

phenomenologically when he assumed the spins to return to equilibrium exponentially. At thermal equilibrium before any energy is introduced into the system, the spins populate the two levels approximately according to the Boltzmann distribution

$$\frac{\eta_+}{\eta_-} = e^{-\Delta E/kT} \tag{2-11}$$

where η_+ represents the concentration of electron spins in the upper (or parallel to H_o) level and η_- the lower level population, k is Boltzmann's constant, T the absolute temperature and ΔE the energy splitting of the levels given in Equation (1-5).

At thermal equilibrium the lower energy level is more densely populated, and since absorption and induced emission are equally probable, in order to observe net absorption of energy the system must remain near thermal equilibrium.

If the static magnetic field in the z-direction is given by $\vec{H} = H_o \hat{k}$, and the static magnetization is given by $\vec{M}_o = \chi_o \vec{H}_o$ where χ_o is the static magnetic susceptibility, then Bloch assumed the rate of change of the magnetization in the z-direction to be

$$\frac{d M_z}{d t} = -\frac{(M_z - M_o)}{T_1} \tag{2-12}$$

where M_z is the instantaneous z-component of the magnetization and T_1 is the longitudinal or spin-lattice relaxation time. The rate of change of the x- and y-component of the magnetization is given by

$$\begin{aligned} \frac{d M_x}{d t} &= -\frac{M_x}{T_2}, \text{ and} \\ \frac{d M_y}{d t} &= -\frac{M_y}{T_2}, \end{aligned} \tag{2-13}$$

where T_2 is the transverse or spin-spin relaxation time.

When the alternating microwave field

$$\vec{H}_r = H_1 (\hat{i}' \cos \omega t + \hat{j}' \sin \omega t)$$

is applied, then the total rate of change of the components of the magnetization are given by

$$\frac{d M_z}{d t} = \frac{M_o - M_z}{T_1} + \gamma (\vec{M} \times \vec{H})_z \quad (a)$$

$$\frac{d M_x}{d t} = \gamma (\vec{M} \times \vec{M}_r)_x - M_x/T_2 \quad (b) \qquad (2\text{-}14)$$

$$\frac{d M_y}{d t} = \gamma (\vec{M} \times \vec{H}_r)_y - M_y/T_2. \quad (c)$$

Equations (2-14) are known as the Bloch equations.

The solution of Bloch's equations are given in numerous papers on both nuclear and electron spin resonance (39, 45). Therefore, the results will be stated and discussed.

If the static magnetic field is $H_o \hat{k}$ and the alternating field is applied in the x-direction, then the solution to the Bloch equations is found by transforming to a rotating coordinate system about the z-axis and solving for $M_{x'}$, $M_{y'}$ and $M_{z'}$ in the rotating system. The solutions that will be given are for slow passage through resonance. In slow passage the rate at which $\vec{H}_o$ is swept through resonance is long compared to the relaxation time; therefore, the magnetization maintains its equilibrium value. The components of magnetization during slow passage can be considered as being almost constant in the rotating system, therefore,

$$\frac{d M_{x'}}{d t} = \frac{d M_{y'}}{d t} = \frac{d M_{z'}}{d t} = 0 .$$

By transforming the solution back into the laboratory frame of reference, it is found that

$$M_z = \chi_o H_o \frac{1 + T_2^2 (\omega_o - \omega)^2}{1 + T_2^2 (\omega_o - \omega)^2 + \gamma^2 H_1^2 T_1 T_2}, \qquad \text{(a)}$$

and (2-15)

$$M_x = \tfrac{1}{2} \chi_o \omega_o \frac{T_2^2 (\omega_o - \omega)(2 H_1 \cos \omega t + 2 H_1 \sin \omega t)}{1 + T_2^2 (\omega_o - \omega)^2 + \gamma^2 H_1^2 T_1 T_2} \qquad \text{(b)}$$

where $\omega_o = \gamma H_o$ is the resonance frequency.

The in phase and out of phase components of M_x with respect to the alternating field can be expressed by writing M_x in complex form given by

$$M_x = \chi^* \cdot 2 H_1 e^{j\omega t} \qquad (2\text{-}16)$$

where χ^* is the complex susceptibility given by Equation (2-10) and the alternating field is the real part of $2 H_1 e^{j\omega t}$. The x-component of the magnetization can then be written as the real part of Equation (2-16), hence,

$$M_x = \chi' 2 H_1 \cos \omega t + \chi'' 2 H_1 \sin \omega t. \qquad (2\text{-}17)$$

Equations (2-15) and (2-17) can be combined to give the components of the susceptibility. The susceptibilities are

$$\chi' = \tfrac{1}{2} \chi_o \omega_o \frac{T_2^2 (\omega_o - \omega)}{1 + T_2^2 (\omega_o - \omega)^2 + \gamma^2 H_1^2 T_1 T_2} \qquad \text{(2-18a)}$$

and

$$\chi'' = \tfrac{1}{2}\,\chi_o\,\omega_o\,T_2\,\frac{1}{1 + T_2^{\,2}\,(\omega_o - \omega)^2 + \gamma^2\,H_1^{\,2}\,T_1\,T_2} \qquad (2\text{-}18b)$$

In discussing Equations (2-18), there are two conditions that will be considered. They are as follows:

(1) The alternating field amplitude is such that $\gamma^2\,H_1^{\,2}\,T_1\,T_2 \ll 1$. The z-components of the magnetization is approximately equal to the static magnetization $\chi_o\,H_o$, or in other words the spin-lattice relaxation time is sufficiently short to maintain the Boltzmann distribution of the levels. The frequency dependence of the susceptibilities as a function of $(\omega_o - \omega)\,T_2$ is shown in Figure 2.

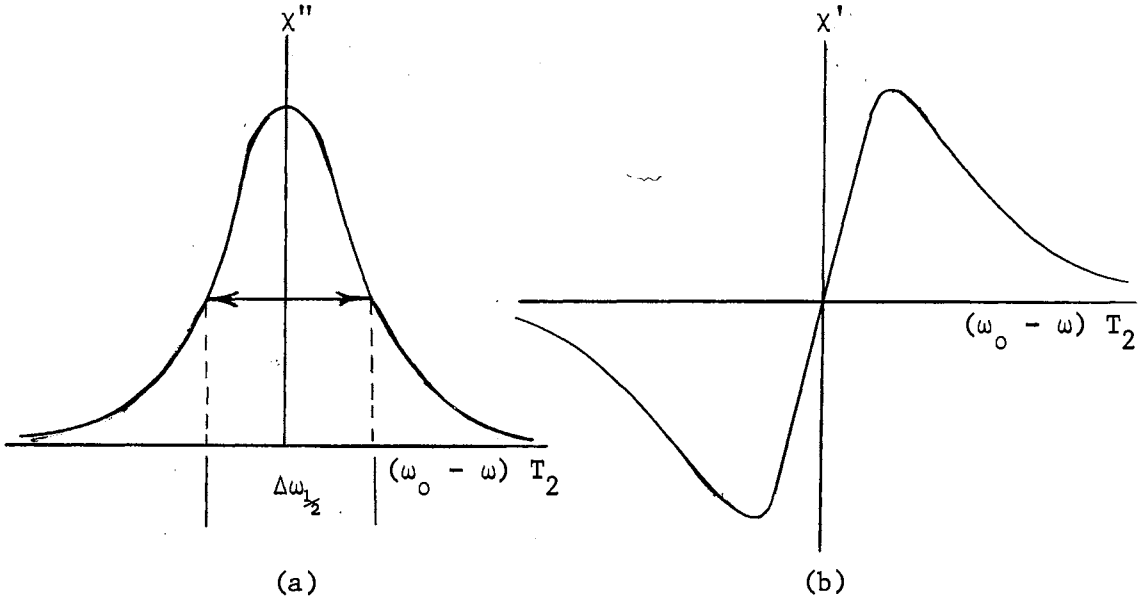

Figure 2. (a) The Imaginary Part, χ'', of the Complex Susceptibility as a Function of $(\omega_o - \omega)\,T_2$. (b) The Real Part, χ', of the Complex Susceptibility. Both are for the Condition $\gamma^2\,H_1^{\,2}\,T_1\,T_2 \ll 1$.

It should be noted that the absorption line width at half intensity $\Delta \omega_{\frac{1}{2}}$ is determined by the spin-spin relaxation time and $\Delta \omega_{\frac{1}{2}} = 1/T_2 = \gamma \Delta H_{\frac{1}{2}}$. This is one form of homogeneous broadening.

(2) When $\gamma^2 H_1^2 T_1 T_2$ is of the order of unity or greater. This is the case of saturation of the spin system. The spin-lattice relaxation cannot carry the absorbed power away fast enough to maintain equilibrium. As H_1 is increased, χ'' and χ' will become weaker and eventually broaden out completely.

It should be noted that the power absorbed from the alternating field depends on the absorptive (or out of phase) component of the susceptibility and is given by

$$P = \frac{\omega}{2\pi} \int_0^{(\frac{\omega}{2\pi})} \cdot (\frac{d\vec{M}}{dt})\, dt = \tfrac{1}{2}\, \omega\, \chi''\, H_1^2 . \qquad (2\text{-}19)$$

Crystalline Field Theory

Introduction

For the case of a free ion the general Hamiltonian is given by

$$H = V_F + V_{LS} + V_{SS} + V_N + V_Q + V_H + V_h, \qquad (2\text{-}20)$$

where V_F is the coulomb interaction term, V_{LS} is the spin-orbit interaction, V_{SS} is the spin-spin interaction, V_N is the magnetic dipole-dipole interaction between the nucleus and electronic magnetic moments, V_Q is the quadrapole interaction, V_H is the interaction with the external magnetic field and V_h is the interaction of the nucleus with the external field (46). However, the influence of the surrounding crystalline field has not been taken into consideration. The interaction potential of the

crystalline field will be denoted V_c.

The field distribution of the static crystalline field is calculated by assuming the surrounding ions as point charges or point dipoles located at the lattice points. Therefore, the ion is in a Stark field with the symmetry determined by the static charges.

If the surrounding ions are considered not to interact with the paramagnetic center, then the potential V_c obeys Laplace's equation. The solutions are generalized Legendre polynomials. V_c can be expanded using the polynomials, and the symmetry of the fields are applied to terminate the expansions.

The magnitude of the crystalline field is classified as strong, medium, and weak. The classifications are considered relative to the other interaction terms of the Hamiltonian. In the case of a weak field the crystalline field can be introduced as a perturbation. For medium fields the perburbation theory is applied before V_{LS} is calculated. Also the quenching of the orbital angular momentum is common. The strong fields usually correspond to covalent bonding. Therefore, the strength of the crystalline field determines at what point the crystal field perturbations are introduced. In the treatment of the crystalline field as a perturbation the operator-equivalent method is applied to find the matrix elements of the potentials (46, 47).

Kramer's Degeneracy and the Jahn-Teller Theorem

Kramer's theorem assures that when an ion with an odd number of electrons is in the presence of an electric field having some degree of symmetry at least a twofold degeneracy will exist. The Kramer's degeneracy can be lifted by applying a magnetic field. Paramagnetic resonance

corresponding to transitions between these levels can be observed.

A second theorem of particular interest is the Jahn-Teller Theorem. The theorem states that if a non-linear molecule of a given symmetry has a degenerate ground state, that the state will be unstable and nuclear displacements will distort the molecule so as to lift the degeneracy. The same should hold for an ion in a crystal.

Spin Hamiltonian Formalism

The magnetic fields that would be created at the ion nucleus by the orbital motion of the unpaired electrons would be so great compared to the externally applied fields that they would be completely dominant. However, this is not the case. The electron spin associated with the paramagnetic centers in single crystals are many times found to be closely related to the spin of a free electron with g-factor of 2.0. This is referred to as quenching of orbital angular momentum. Since the spin angular momentum is predominant, the properties of the paramagnetic centers can be incorporated into an effective spin Hamiltonian. The parameters of the spin Hamiltonian, such as the g-factors in the principal axis system, the initial splittings and the hyperfine constants, are determined experimentally. A model of the crystal field is postulated which will correspond to the spin Hamiltonian and explain the observed parameters. The spin Hamiltonian is simply a description of the experimental results.

As stated earlier, in the case when the orbital angular momentum is quenched the magnetization can be treated as though it originates from spin alone. The spin Hamiltonian formalism is based on the definition of an effective spin $\vec{S}'$. The effective spin is chosen so that $2S' + 1$

equals the number of experimentally observed Zeeman transitions. The eigenfunctions which correspond to the $2S' + 1$ levels are considered to be pure spin states even though they are actually a mixture of crystal field and spin-orbit effects. S' is a fictitious spin and it will be denoted as S.

The spin Hamiltonian is generally written in the form,

$$H = H_{st} + H_{so} + H_{ss} + H_z + H_{hf} + H_Q + H_n, \qquad (2\text{-}21)$$

where the terms are the following,

H_{st}, the crystalline field interaction

H_{so}, the spin-orbit interaction

H_{ss}, the spin-spin interaction

H_z, the Zeeman interaction

H_{hf}, the electron-nuclear dipole interaction, or hyperfine interaction

H_Q, the electron-nuclear quadrupole interaction

H_n, the nuclear Zeeman interaction.

H_z, H_{st} and H_{so} involve energies which are too large for excitation by microwave energies. H_Q and H_n involve interaction which are not of importance for the particular paramagnetic center under investigation in this study so they will not be discussed in detail.

The spin Hamiltonian which characterizes the ESR spectrum in this study consists of only the two terms H_z and H_{nf}.

However, a brief mention of the spin-orbit term H_{so} is in order since it can contribute to shifts in the g-value of the resonance.

As stated earlier, for a free ion the orbital angular momentum and the spin angular momentum are coupled together (Russell-Sanders coupling) to give a new quantum number $\vec{J} = \vec{L} + \vec{S}$, where $\vec{J}$ is a good quantum number for low external magnetic fields. The g-factor is given by the Lande g-factor given in Equation 1-2. A classical calculation of the field the electron would see is in the order of magnitude of 600,000 oersted. However, in the presence of a symmetric crystalline field the spin-orbit interaction is quenched.

The spin-orbit coupling term is generally written in the form

$$H_{so} = \lambda \vec{L} \cdot \vec{S} \qquad (2\text{-}22)$$

where $\vec{L}$ is the orbital angular momentum and λ is called the spin-orbit coupling constant.

The case where the crystalline field potential is much larger than the spin-orbit coupling constant is the only case that will be considered. For this case, another interaction term is considered, that being $\beta \vec{H}_o \cdot \vec{L}$, where β is the Bohr magneton. It is usually treated in simpler cases as a perturbation on the larger $\lambda \vec{L} \cdot \vec{S}$ term. However, neither term gives a first order contribution. The $\beta \vec{H}_o \cdot \vec{L}$ term does induce some small orbital circulation. The spin will therefore experience a small induced field due to the small net circulation of the orbital motion.

In summary, the g-shift arises because of the interplay between the spin-orbit and orbital Zeeman interactions. The spin experiences both the applied magnetic field and an induced magnetic field. A phenomena involving the effects of two interactions of this nature can be considered as an application of a generalized form of second-order

perturbation theory. If the two terms $\lambda \vec{L} \cdot \vec{S}$ and $\beta H_o \cdot L$ are added as small perturbations to the Hamiltonian they can produce a fine structure term for ground states of spin greater than one half. The fine structure terms will be discussed in more detail later.

For a very pellucid discussion of the effects of the spin-orbit interactions with an example worked out in detail refer to the text by Slichter (41).

The Zeeman Term

The spectroscopic splitting factor or g-value given by the resonance equation $h\nu = g \beta H_o$ is a real, second rank, symmetric tensor which can be written in the form,

$$\vec{g}' = \begin{pmatrix} g'_{xx} & g'_{xy} & g'_{xz} \\ g'_{yx} & g'_{yy} & g'_{yz} \\ g'_{zx} & g'_{zy} & g'_{zz} \end{pmatrix} \qquad (2\text{-}23)$$

where $g'_{ij} = g'_{ji}$.

However, since this matrix is Hermitian, a similarity transformation can be choosen to diagonalize the matrix. The g-tensor can then be written as

$$\vec{g} = \begin{pmatrix} g_1 & 0 & 0 \\ 0 & g_2 & 0 \\ 0 & 0 & g_3 \end{pmatrix} \qquad (2\text{-}24)$$

It should be noted that the magnetic axes which correspond to the diagonalized g-tensor will not in general be coincident with the crystal-

line axes of the host crystal.

The g-tensor is very commonly written in the dyadic form

$$\vec{g} = \hat{i}\, g_1\, \hat{i} + \hat{j}\, g_2\, \hat{j} + \hat{k}\, g_3\, \hat{k}, \tag{2-25}$$

where $\hat{i}$, $\hat{j}$, $\hat{k}$ are the unit vectors for the coordinate system which diagonalizes the g-tensor.

If the external magnetic field $\vec{H}_o$ is given by

$$H_o = H_x\, \hat{i} + H_y\, \hat{j} + H_z\, \hat{k}, \tag{2-26}$$

then the Zeeman term of the spin Hamiltonian is given by

$$H = \beta\, \vec{H}_o \cdot \vec{g} \cdot \vec{S}. \tag{2-27}$$

The quantity $\vec{H}_o \cdot \vec{g} = H_x\, g_1\, \hat{i} + H_y\, g_2\, \hat{j} + H_z\, g_3\, \hat{k}$ is a vector which may vary in both direction and magnitude from $\vec{H}_o$, and therefore it can be thought of as the effective magnetic field seen by the electron.

If x_1, x_2, and x_3 are the three mutually orthogonal directions which correspond to the principal components g_1, g_2, and g_3 of the g-tensor respectively, then the effective value of g in the direction of $\vec{H}_o$ is given by

$$g = [g_1^2 \cos^2 \phi_1 + g_2^2 \cos^2 \phi_2 + g_3^2 \cos^2 \phi_3]^{\frac{1}{2}}, \tag{2-28}$$

where ϕ_1, ϕ_2, and ϕ_3 are the angles between the external field H_o and x_1, x_2, and x_3 respectively.

For systems of spin where $S \geq 1$, there is sometimes an additional splitting of the levels when the external field is zero. This is caused

by the Stark effect of the surroundings. This term is called the "fine structure" term. For an axially symmetric center along the z-axis the external field $\vec{H}_o$ parallel to z, the fine structure term can be written as

$$H = g_z \beta H_o S_z + D \{S_z^2 - \frac{1}{3} S(S+1)\} \qquad (2\text{-}29)$$

where D is called the fine structure constant. For a more complete discussion of the fine structure refer to Pryce (48) and Abragam and Pryce (49).

The Hyperfine Coupling Term

The hyperfine interaction term is a coupling of the magnetic moment of the unpaired electron spin and the magnetic moment of the nucleus. However, a distinction must be made between an electron in an s-state and one which is in a non s-state.

Consider the non s-state first. The wavefunctions for these states vanish at the nucleus. This means that the interaction can be considered as two dipoles which are separated by a distance $\vec{r}$, where the Hamiltonian term is given by

$$H_1 = \frac{\gamma_e \gamma_n h^2}{r^3} \left[\frac{3(\vec{I}\cdot\vec{r})(\vec{S}\cdot\vec{r})}{r^2} - \vec{I}\cdot\vec{S}\right]. \qquad (2\text{-}30)$$

I is the spin quantum number of the particular nucleus involved and γ_n is the nuclear gyromagnetic ratio.

In the case of an electron in an s-state, the electron wavefunction is non-zero at the nucleus. For these close distances the dipole approximation is given by

$$H_2 = \frac{8\pi}{3} \gamma_e \gamma_n h^2 \vec{I} \cdot \vec{S} \, \delta(\vec{r}), \tag{2-31}$$

where $\delta(\vec{r})$ is the Dirac delta function, which is zero everywhere except at the nucleus. This term is usually called the Fermi contact term.

Since a knowledge of the true electron wavefunction (which is generally a mixture of s-states and non s-states) is generally not known, both terms are included in a linear combination of terms of $\vec{S}$ and $\vec{I}$ given by

$$\sum_{i,j=1,2,3} A_{ij} S_i I_j, \tag{2-32}$$

where A_{ij} is a component of an unknown real, second rank tensor which is determined experimentally.

As in the case of the g-tensor, the A-tensor can also be diagonalized giving

$$\vec{A} = \begin{pmatrix} A_1 & 0 & 0 \\ 0 & A_2 & 0 \\ 0 & 0 & A_3 \end{pmatrix}. \tag{2-33}$$

In general, the principal axes which diagonalize the A-tensor do not correspond to the same set of axes which diagonalize the g-tensor.

If A_1, A_2 and A_3 lie in the y_1, y_2, and y_3 directions respectively, the effective value of $\vec{A}$ in the direction of $\vec{H}_o$ can be written as

$$A = [A_1^2 \cos^2 \Phi_1 + A_2^2 \cos^2 \Phi_2 + A_3^2 \cos^2 \Phi_3]^{\frac{1}{2}} \tag{2-34}$$

where Φ_1, Φ_2, Φ_3 are the angles the external field $\vec{H}_o$ makes with y_1, y_2 and y_3 respectively.

Using the dyadic notation, the hyperfine term can now be written as

$$H_{hf} = \vec{I} \cdot \vec{A} \cdot \vec{S} \qquad (2\text{-}35)$$

Combining Equations (2-27) and (2-35), one has more general Hamiltonian

$$H = \beta \vec{H} \cdot \vec{g} \cdot \vec{S} + \vec{I} \cdot \vec{A} \cdot \vec{S} \qquad (2\text{-}36)$$

which is the form of the Hamiltonian which characterizes the ESR spectrum that is the object of this study.

If the nucleus which the electron is associated with has a nuclear spin $\vec{I}$, then it is quantized into $2I + 1$ allowed orientations in the presence of an external magnetic field. These $2I + 1$ allowed orientations of the nucleus are those for which the projections I_z on the external magnetic field are given by $I_z = M_I \hbar$, $M_I = I, I-1, I-2, \ldots, -I$, where M_I is called the nuclear spin quantum number. Therefore, the effective magnetic field seen by the unpaired electron depends in which one of the $2I + 1$ states in which the nuclear spin is oriented. The absorption occurs only when the spin changes orientation relative to $\vec{H}_o$ without a simultaneous change in the nuclear orientation. This is usually stated in terms of selection rules for allowed ESR transitions. These rules are $\Delta M_s = \pm 1$ and $\Delta M_I = 0$.

The selection rules are a consequence of the conservation of energy and angular momentum. With the above two selection rules, when the system undergoes a transition from $m_s = -\frac{1}{2}$ to $m_s = +\frac{1}{2}$ a photon of energy $h\nu = g \beta H_o$ is absorbed, and the spin angular momentum changes only by an amount $\hbar$, which is the unit of angular momentum of the photon absorbed from the electromagnetic field.

In order to better understand the effects of some of the interaction terms of the Hamiltonian on the energy level of a free ion when it is placed in a symmetric crystalline environment, consider the example given in Figure 3. The free ion is first placed in a crystalline field of high symmetry. This removes the five-fold orbital degeneracy and splits the energy level into a doubly and triply degenerate level. If the example is thought of as an electron in a d-orbital, the T_d symmetry field will produce this splitting of the free ion energy level. However, it should be noted that the splitting will probably be on the order of 10^4 cm^{-1}, which is much greater than the microwave energy. If the symmetry of the field is reduced, the two levels are split into three singly degenerate and one doubly degenerate level. A crystalline field of D_{4h} symmetry will produce this splitting. Again the energies involved between these levels are much greater than the microwave energies. The next interaction shown is the spin-orbit interaction. Note that the spin-orbit interaction splits the orbital doubly degenerate level. An external magnetic field is next applied to lift the spin degeneracy. Only the ground state is shown completely. The effects of a nuclear spin of $I = 1$ is then included. The spin levels are split into three levels as a result of the hyperfine interaction. These levels correspond to the $2I + 1$ orientations of the nuclear moment in the external magnetic field. The hyperfine interaction is shown only for the ground state of the ion. The allowed transitions, $\Delta M_I = 0$ and $\Delta M_s = \pm 1$, are shown by the dotted arrows. Energies from 10^{-1} cm^{-1} to 10^{-3} cm^{-1} are typical of the hyperfine interaction term.

For a more detailed description of the other terms in the spin Hamiltonian the review articles by Bleaney and Stevens (50), and Bowers

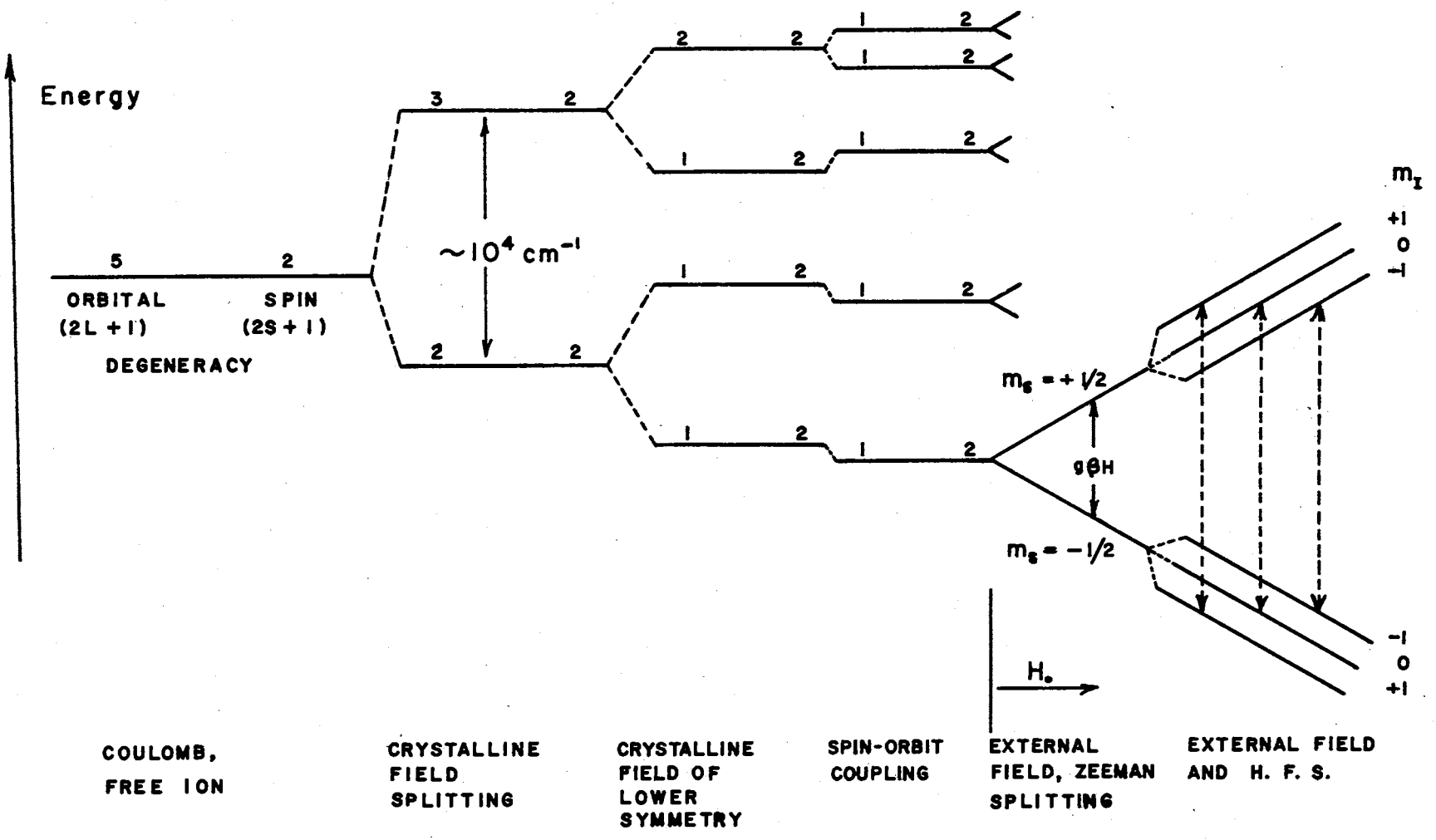

Figure 3. Effects on the Energy Level of an Electron From Various Interactions in a Crystalline Environment

and Owen (51), and also the text by Low (46) should be consulted.

The Breit-Rabi Expression

Using Equation (2-36) for the spin Hamiltonian, the allowed energy levels can be calculated. Breit and Rabi (52) calculated these levels for the case of an isotropic g-tensor and an isotropic A-tensor. For the case of $S = \frac{1}{2}$, the energy for the allowed transitions $\Delta M_s = \pm 1$, $\Delta M_I = 0$ are, neglecting terms greater than second order in $A/g\beta H$,

$$h\nu = g\beta H + M_I A + \frac{A^2}{2g\beta H}\left[I(I+1) - M_I^2\right] \qquad (2\text{-}37)$$

for $m_I = I, I-1, \ldots, -I$. Since the ESR experiments are performed at constant frequency it is convenient to solve Equation (2-37) explicitly for the external magnetic field H, thus

$$H = \frac{1}{2g\beta}\left[(h\nu - M_I A) + \sqrt{(h\nu - M_I A)^2 - 2A^2\left[I(I+1) - M_I^2\right]}\right] \qquad (2\text{-}38)$$

As stated earlier, this expression was derived by initially assuming that the $\vec{g}$ and $\vec{A}$ tensors to be isotropic. In order for this expression to be used the variation of both $\vec{g}$ and $\vec{A}$ will have to be small. In this study the variation of $\vec{g}$ and $\vec{A}$ are small enough so that the value of g for a particular orientation can be obtained by using Equation (2-28) and the value of A can be obtained by using Equation (2-34). The justification for the use of Equation (2-38) in this study will be duscussed in more detail later.

CHAPTER III

INSTRUMENTATION

Basic ESR Spectrometer

In order to produce electron spin resonance, a spectrometer that operates in the x-band region of the microwave spectrum was used for this study. In order to produce resonance in this region of the microwave spectrum a magnetic field of several thousand oersted is required.

In Chapter II the condition required to produce resonance was outlined. In this chapter the particular instrumentation used in this research to create the resonance condition and to detect and display the resonance signal will be outlined. A brief discussion of the functions of the different components of the spectrometer will also be given along with the description of the equipment.

The spectrometer used in this research is a microwave bridge spectrometer which utilizes a reflection cavity. The spectrometer was constructed mainly by Dr. M. D. Bell (53) using fundamental ESR design techniques. The spectrometer can be considered to be comprised of several basic components as given in Figure 4. The components are as follows:

(1) A stabilized source of microwave energy.

The microwave energy is provided by a Varian reflex klystron, VA201B, which produces about 100 milliwatts of power. The voltage supply for the klystron is a commercial power supply. A modified Pound

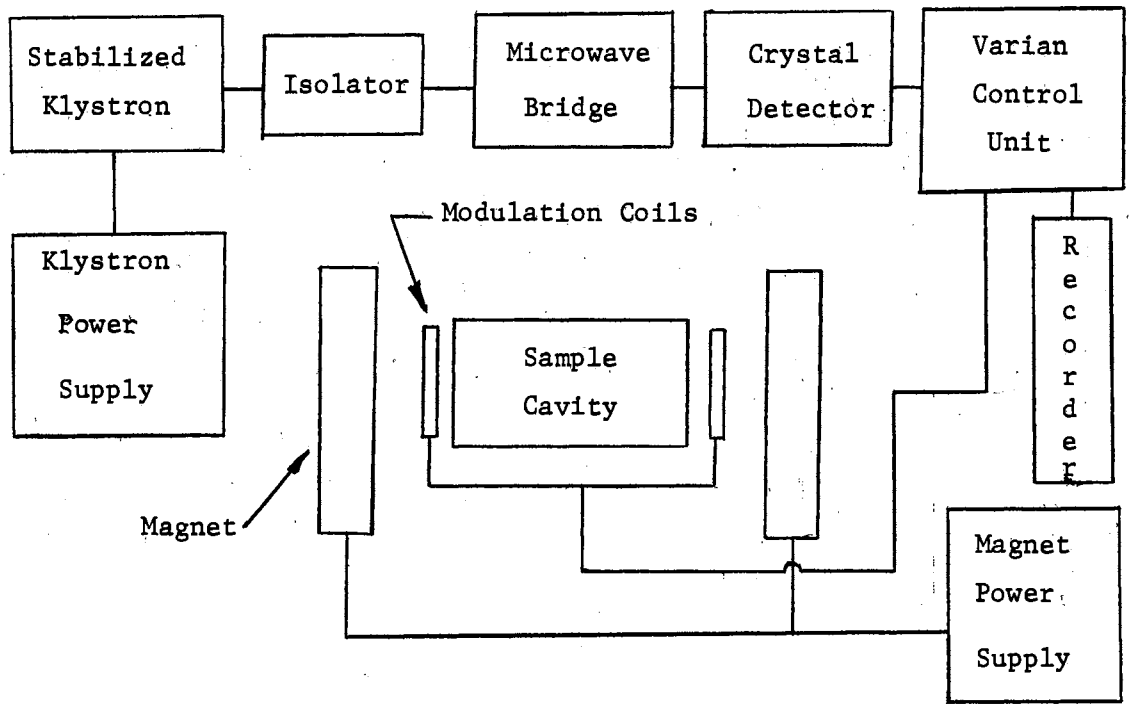

Figure 4. The Basic Components of an ESR Bridge Spectrometer

stabilization circuit is used to stabilize the klystron. The klystron is isolated from vibrations, as is the entire spectrometer, by vibration free supports, and it is thermally isolated in a water cooled silicone oil bath.

(2) The microwave bridge. The bridge is isolated from the stabilized klystron by a ferrite unidirectional isolator. The isolator keeps microwave energy from being reflected back into the stabilizing system and the klystron. The bridge (see Figure 6) consists of two branches. The bridge microwave circuit function is to allow energy to be introduced into the sample cavity and to permit simultaneous monitoring of the reflected energy from the cavity. The energy is introduced into the

two branches by a magic tee. The lower branch contains a precision attenuator and a ferrite circulator. The four port circulator enables the energy introduced into the first port to be channeled out of the adjacent second port only; hence, the energy is directed to the cavity. The reflected energy from the cavity travels back into the second port, is then channeled through the third port only, and hence to the crystal detector. The upper branch provides a microwave reference or bias signal to the detector.

(3) A varian 6" electromagnet, Model A 4007-1, with its power supply. The magnet produces a sufficiently homogeneous magnetic field. The magnet has a mechanical linear field sweep which enables the field to be swept through the resonance line.

(4) A magnetic field modulation system which superimposes a small 100 kc field on the large polarizing field of the Varian 6" magnet. The modulating field is introduced by coils mounted on the sides of the resonance cavity.

(5) A signal detection system. The signal is monitored from the bridge, using either a silicon crystal diode detector or twin bolometer detectors. The modulation field introduced enables ac amplifiers and a phase sensitive detector to be employed in the signal detection. A Varian 100 kc crystal oscillator and a modulation amplifier to drive modulation coils is contained in the Varian modulation and control unit.

(6) A sample cavity with a variable dielectric coupling to the waveguide. The sample cavity is connected to the waveguide with a variable dielectric coupling probe that can be manually adjusted for the desired coupling (54).

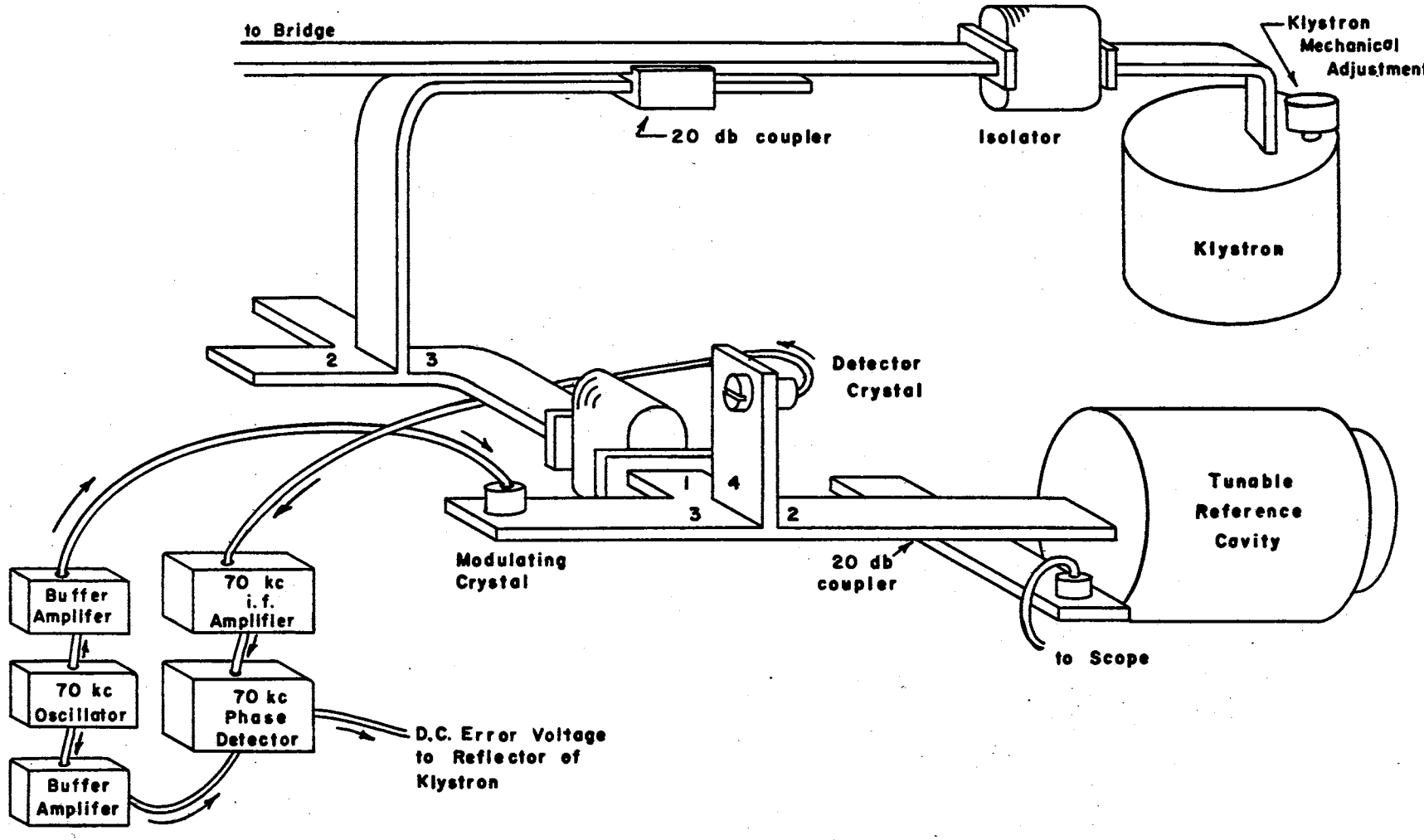

Figure 5. The Modified Pound Frequency Stabilizer

Description and Operation of the ESR Spectrometer Used in the Investigation

Klystron Frequency Stabilization

A modified equal arm Pound stabilization microwave circuit was used exclusively in this research.

To obtain data from a sample and to display the dispersive or the absorptive component of the magnetic susceptibility separately, there must be a stable source of microwaves (55, 56, 57). The modified or "equal arm" discriminator is shown in Figure 5.

The klystron is isolated from the stabilization system by a ferrite isolator. The isolator keeps any reflected power from traveling back into the klystron and upsetting its stability. A 20 db coupler then connects a fraction of the signal power into arm 1, the H-plane arm, of the magic tee. The signal is divided into arm 2 and arm 3 of the tee. The klystron frequency is on the order of 9.1 kmc and will be denoted by ω.

The energy that enters arm 2 is partially reflected and partially absorbed at the reference cavity. The cavity is a silver plated quartz cavity with an adjustable "plunger type" end which can be used to vary its frequency response. The cavity is encased in a thermal jacket.

The cavity is coupled to the waveguide approximately at critical coupling. There will be a 180° phase change on either side of the cavity resonance (58). The reflected power from the cavity will travel into arm 4 of the tee where it is mixed and detected at the crystal detector with the reflected signal from arm 3.

The half of the signal that originally enters arm 3 is mixed with a 70 kc "local oscillator" signal at the modulation crystal. The modula-

tion crystal in arm 3 superimposes the 70 kc oscillator frequency and the microwave frequency to produce two amplitude modulated side bands. The side bands generated are above and below the 70 kc oscillator frequency by an amount equal to the intermediate frequency. Upon reflection from the modulating crystal, the side bands travel to the detector in arm 4 of tee junction. Part of the signal from arm 3 returns to the cavity where it is reflected and produces second-order side-bands frequencies. However, these may be neglected.

At the crystal detector in arm 4 there are three different frequencies incident; the two side bands and the wave reflected from the cavity. The voltage thus produced by the crystal is proportional to the reactive component of the wave reflected from the cavity. Also, since there is a 180° phase change on either side of the cavity resonance, the deviation of the klystron on either side of resonance will therefore affect the phase of the crystal output (59).

The signal thus obtained from the crystal detector is amplified and demodulated using a 70 kc amplifier. The signal is then compared to the 70 kc oscillator in a phase sensitive detector. The detector produces a dc voltage signal with sign depending on which side of the cavity resonance the klystron is operating; and the magnitude depends on the input voltage. The dc "error" voltage is then amplified. After being amplified, the error voltage is applied to the klystron reflector in order to adjust the klystron frequency. Since the klystron reflector voltage operates at a high negative potential, the phase detector cannot operate at ground potential; the phase detector circuit, therefore, must be isolated from the ground potential.

The frequency of the klystron is now essentially "locked" onto the

reference cavity frequency.

The Microwave Bridge Circuit and Detector

The microwave signal travels from the stabilized klystron into the microwave bridge shown in Figure 6. Again the basic function of the bridge is to allow energy to be introduced into the sample cavity and to permit simultaneous monitoring of the reflected energy from the cavity (59).

When the microwave power enters the magic tee through the arm shown in Figure 6, it travels into the upper branch and lower branch of the bridge. The upper branch contains a ferrite isolator, an adjustable ferrite phase shifter, and an adjustable attenuator. The signal from this branch is used to maintain a bias voltage on the detector crystal by adjusting the bias attenuator and the phase of this bias or reference signal can be controlled by use of the bias phase shifter. The adjustment of the phase of this reference signal will determine whether the bridge is going to be sensitive to the dispersive or the absorptive component of the magnetic susceptibility.

The other half of the signal travels into the lower branch of the bridge. The amount power to be introduced into the sample cavity is controlled using the variable power attenuator. The signal enters the folded tee and then enters the four port microwave ferrite circulator which is described in detail in literature (60). Briefly, power entering one port of the circulator will exit only from the adjacent port. The signal entering the circulator travels into the arm containing the slide-screw tuner and sample cavity. Power is reflected back into the circulator from both the slide screw tuner and the sample cavity. From

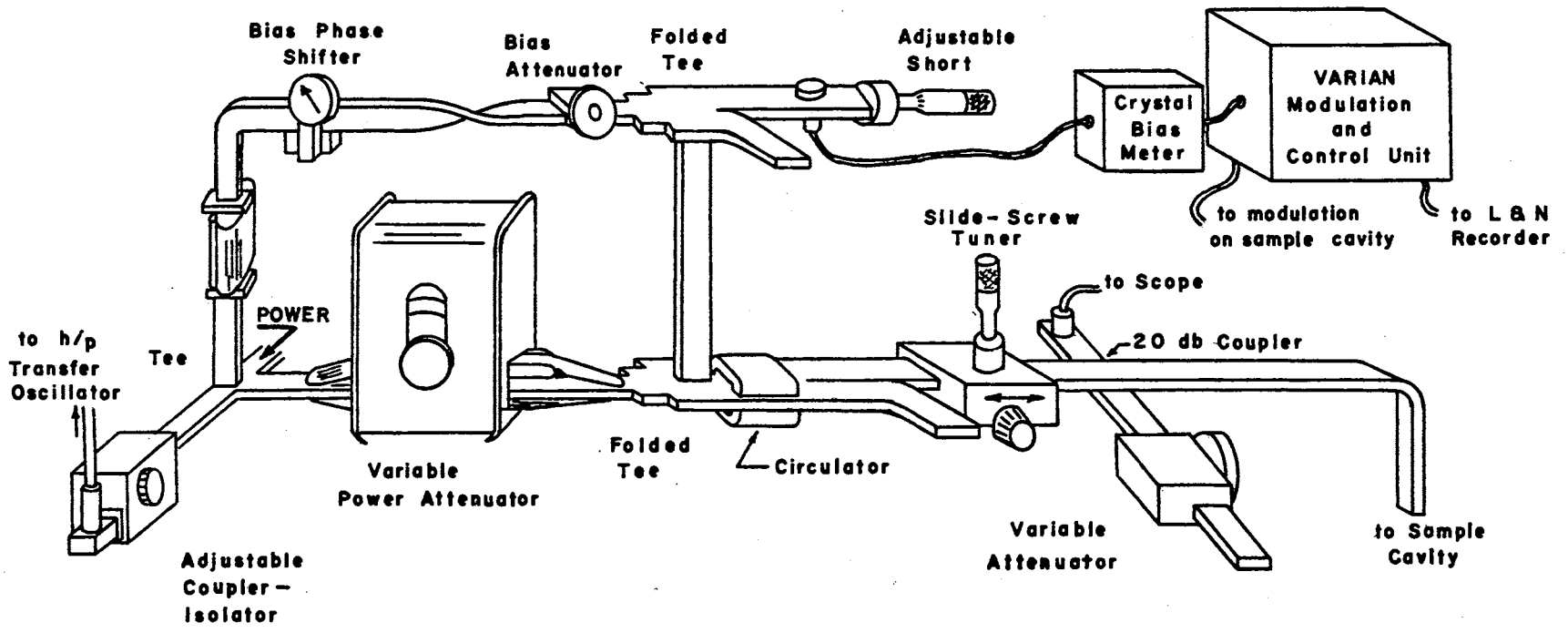

Figure 6. The Microwave Bridge and Detector.

the circulator it travels back into the folded tee where part of the signal travels up the vertical arm into the folded tee in the upper or reference branch of the bridge. Therefore, the crystal detector receives three signals: one is the reference signal from the reference branch of the bridge; the second is the reflected signal from the slide-screw tuner, and the third is the reflected signal from the sample cavity. Since the Varian model V-4560 modulation and control unit is a phase sensitive detector, the bridge must be "balanced" as closely as possible.

The phase detector locks onto the continuous input signal. As the external magnetic field is swept through resonance, the amplitude of the 100 kc signal superimposed on the microwave carrier signal reflected from the cavity will vary in amplitude depending on the shape of the absorption curve and will undergo a 180° phase change as H_o is swept through the absorption maximum. This is more easily seen in Figure 7.

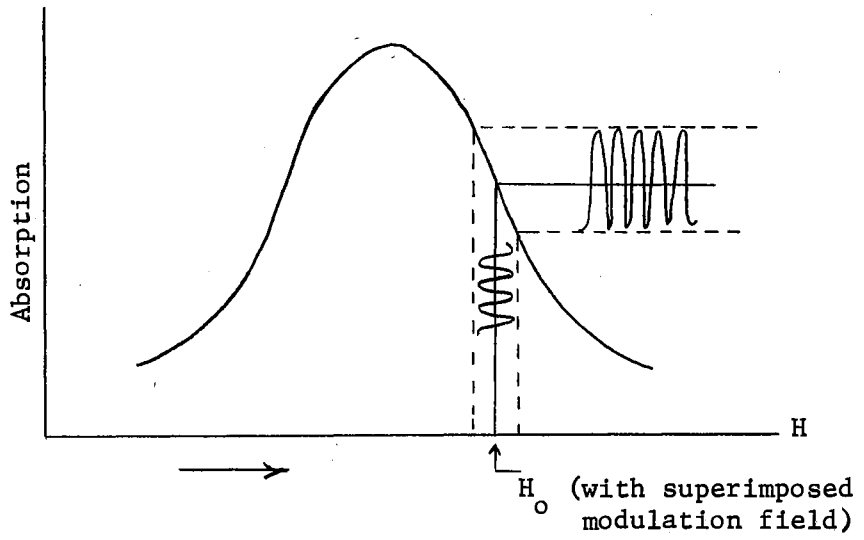

Figure 7. The 100 kc/sec Modulation Amplitude Dependence at Resonance

The Varian phase detector or control unit consists of a 100 kc amplifier demodulator, a 100 kc crystal oscillator which acts as a reference for the phase "lock-in" detector and provides the 100 kc modulation frequency to the modulation coils, and a rectification integrator circuit from which the signal is sent to the graphic recorder. The signal produced by this detection system will be the first derivative of the actual absorption curve. The relationship between the phase of the 100 kc reference oscillator in the Varian control unit and the 100 kc modulation frequency can be be varied. For this study the control unit was operated with these two frequencies either in phase or in quadrature with respect to each other. This should not be confused with the selection of the mode of operation of the spectrometer for either the dispersive or absorptive modes by adjustment of the bias phase shifter.

A much more complete description of phase lock-in detectors and microwave bridge operation can be found in the book by Poole (61).

Magnetic Field Modulation

Instead of measuring a dc detector output using dc amplifiers, a sinusoidal, 100 kc, modulation field is superimposed on the static magnetic field H_o as it is swept through resonance. This enables AC amplifiers which are much more stable to be used. This helps reduce the signal-to-noise ratio. Thus, when the microwave frequency and the modulation frequency are superimposed, the desired power absorption information will be incorporated into the modulation envelope of the microwave or carrier signal. The amplitude of the modulation signal can be varied from .01 oersted to 10.0 oersted. The selection of the proper amplitude must be chosen with regards to the line width of the particular

sample's absorption.

The choice of the modulation frequency is not critical; however, several effects must be considered. When a crystal detector is employed, it introduces a crystal noise voltage that is proportional to $1/\Delta f$, since the noise power of a crystal rectifier varies as $\Delta f/f$, where Δf is the band width of the given modulation frequency f. The noise voltage is shown in Figure 8.

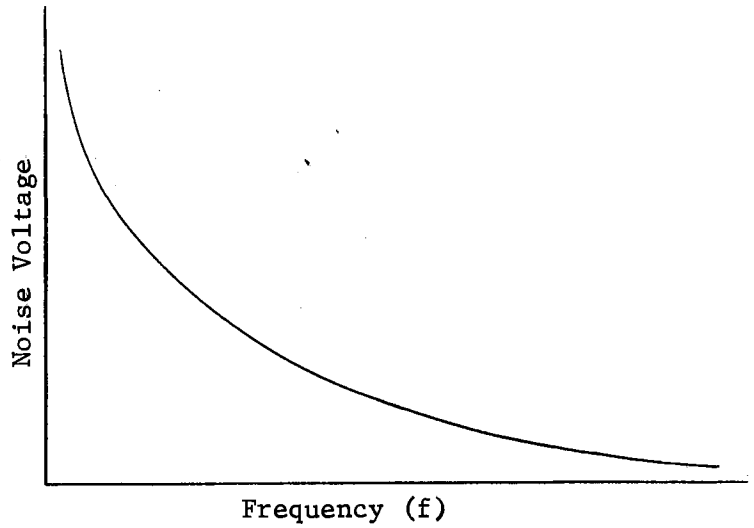

Figure 8. The Characteristic Noise Spectrum of a Crystal Diode Detector

A very large modulation frequency would therefore seem most desirable. However, for frequencies much higher than 100 kc, the walls of the cavity attenuate the signal. The larger frequencies are also desirable since the magnetic field can be swept through resonance faster without decreasing the signal to noise ratio since the amplifier circuit

can have shorter time constants because of the possible increase in the band width. Another reason for larger modulation frequencies arises because of the possibility of modulation broadening of the absorption line if the modulation frequency is large with respect to the line width.

The Electromagnet System

The magnet used in the spectrometer is a Varian 6 inch electromagnet, Model 4007-1, with its own regulated power supply. The magnet can be rotated 200° about its vertical axis. This enables orientation studies to be made without remounting the crystal for each crystal orientation. A cylindrical cavity must be used if the magnet is to be rotated. The magnet has 6" ring shim pole pieces with a 2.875" gap.

The Sample Resonance Cavity

A Varian rectangular cavity, Model V4531, was used for the majority of work of this study. The iris of this cavity is located such that it will operate in the TE_{102} mode. The sample is mounted on a quartz rod that can be rotated 360° as shown in Figure 9.

The cavity is coupled to the waveguide using a variable dielectric coupling scheme (54, 62). However, the coupling is not adjusted for critical coupling. Instead the coupling is adjusted so that the cavity is undercoupled. This helps prevent the admixture of the absorptive and and dispersive modes as the field is swept through resonance.

Magnetic Field and Scan Rate Measurements

The magnetic field and the scan rate of the magnetic field is meas-

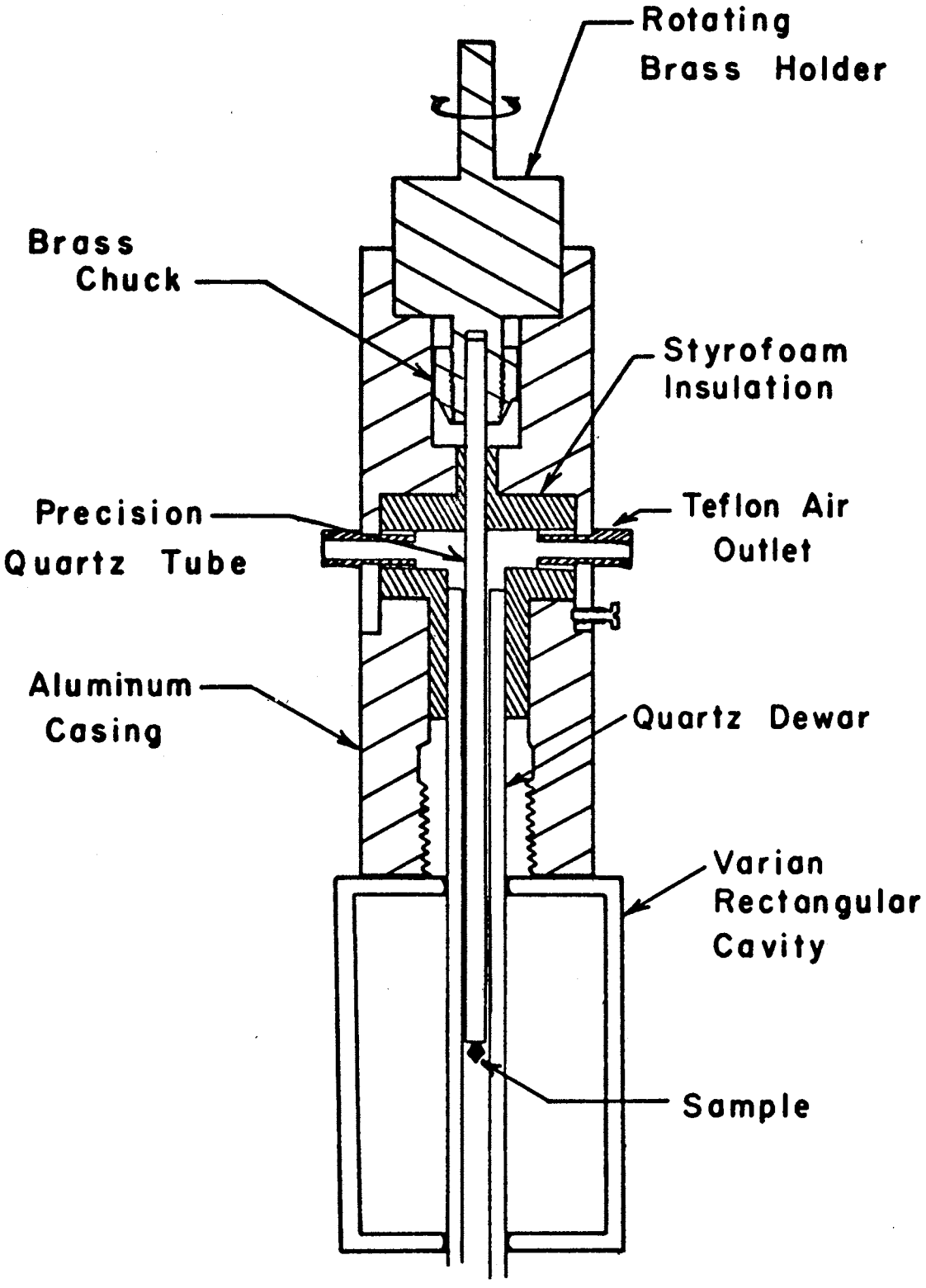

Figure 9. Modified Varian Rectangular Cavity Used for Orientation Study

ured using a nuclear resonance detector. The NMR probe is rigidly supported in the magnetic field with a clamp that fits on the magnet pole piece.[1] The frequency of the NMR oscillator is measured with a h/p 524D electronic counter. The relationship between the magnetic field strength and the NMR oscillator frequency is given by

$$H = \frac{2\pi}{\gamma_p} \nu_p = 2.34868 \times 10^4 \nu_p \text{ (oersted)},$$

where $\gamma_p = 2.67530 \times 10^4$ rad. sec.$^{-1}$ oersted^{-1} is the gyromagnetic ratio of the proton (63).

A magnetic field interval is determined by measuring the scan rate of the magnetic field for that interval. The magnetic field scan rate is linear over the interval. As the field is scanned, the NMR oscillator frequency is measured simultaneously as described above. Markers are placed on the recorder chart at the positions at which the frequency is measured. Several such measurements are made in the interval in which the scan rate is to be measured. The frequency versus the chart displacement (in inches) is plotted. From the slope of the graph the scan rate in oersted/inch can be calculated using the above relation between the magnetic field and the frequency.

A Hewlett-Packard model 540B transfer oscillator is used in conjunction with the 525D counter to measure the klystron frequency. A small amount of the klystron output is monitered as shown in Figure 6.

---

[1] The nuclear magnetic resonance detector is usually abbreviated as the NMR detector for brevity.

CHAPTER IV

RESULTS AND DISCUSSION OF THE STUDY

Introduction to Experimentation

General Remarks on Experimental Observations

The symmetry of the electron spin resonance spectrum of two Type Ib (insulating) diamonds was studied and analyzed. In particular, the symmetry properties of an unusual set of resonance lines in samples D-61 and D-60 were studied in detail. Most of the data were obtained using sample D-61 since it had easily recognizable faces which made it easy to orient. The hyperfine splitting was measured along the principal directions. However, the hyperfine line's intensity was found large enough to detect only in two particular planes of the crystal. The experimental orientation dependence of the hyperfine lines were then compared to the orientation dependence calculated using the Briet-Rabi expression.

Optical absorption measurements in the visible and ultraviolet at room temperature were made on the samples studied.

Laue back reflection X-ray diffraction pictures taken with the X-ray beam parallel to equivalent principal axes of the crystal were found not to be the same. The back reflection spots appeared as streaks which were very pronounced for some of the orientations.

Description of the Diamonds Used in the Study

The unusual electron spin resonance spectrum under consideration in this study was observed in two diamond specimens of our collection which were denoted D-61 and D-60. Both samples have similar physical characteristics. They are both brown with very smooth recognizable flat surfaces, particularly sample D-61 which has two large parallel {110} surfaces. Although {110} faces are not particularly uncommon, most diamonds have {111} faces.

Since the ESR spectrum for the center under consideration in this study is not equivalent when the external magnetic field is parallel to equivalent directions of the crystal, it is necessary to choose a coordinate system to which the orientation dependence can be referred. The majority of the orientation dependence measurements were made on sample D-61. The coordinate system chosen is shown in Figure 10. The [110] axis is directed out of the page of the paper and perpendicular to the (110) plane as shown.

The Orientation Procedure

The diamonds were oriented using a Laue back-reflection X-ray camera. The diamonds were mounted on a goniometer with beeswax and irradiated with X-rays. Using a Greninger net (calibrated for a 3 cm. sample to film distance) the rotations for a desired orientation were determined. The diamonds were then transferred to a precision quartz rod.

The quartz rod was clamped securely in the direction parallel to the direction in which the diamond was mounted. The diamond was then

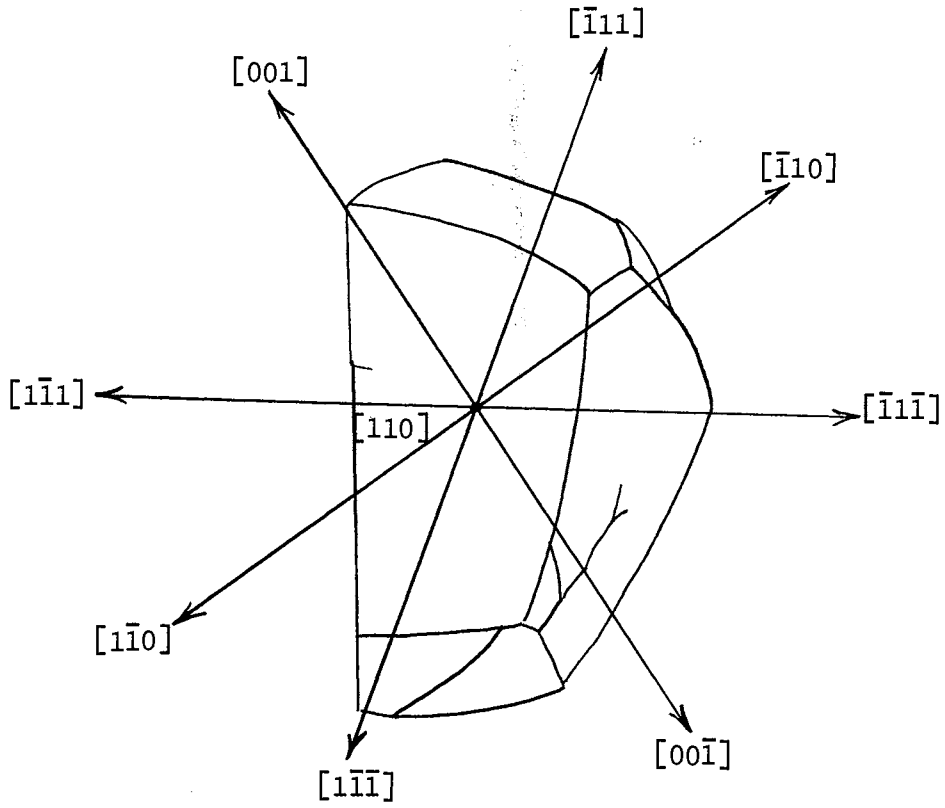

Figure 10. The Coordinate System Chosen for Sample D-61

glued to the quartz rod while still securely held in the beeswax. X-ray pictures of the sample on the quartz rod, after the transfer was made, showed the diamond to be accurately oriented. Also since the samples all had a strong substitutional nitrogen resonance, the orientation was easily verified using the spectrometer.

Orientation Dependence of Previously Observed Nitrogen Resonances in Type I Diamonds

A more detailed review of the orientation dependence of different nitrogen defect centers in diamond is in order since it will be an aid

in understanding the particular model chosen for the center under investigation in this study.

The most commonly observed ESR spectrum in natural, unirradiated, type I diamonds is that arising from substitutional nitrogen donors (25). In the diamond crystal each carbon atom is surrounded by four equally distant nearest neighbor carbon atoms which form a regular tetrahedron. The carbon atoms form covalent bonds with their nearest neighbors. When nitrogen enters the diamond in a substitutional position, the unpaired spin of the donor electron occupies a state which is described as an anti-bonding orbital which is a hybridization of an s- and p-orbital on the main N-C bond direction (64). An extension of approximately 11% from the normal C-C bond length increases the p-characteristic of the hybrid s-p orbital. The electron is thought to be more densely concentrated on the carbon atom than on the nitrogen atom. Because of the increase of the N-C bond length the site symmetry of the substitutional diamond is reduced to a C_{4v} symmetry. It should be noted that the tetrahedral bond direction in the diamond crystal is parallel to the <111> directions. For nitrogen in a substitutional position, the donor electron is localized mainly along the <111> directions and is equally distributed among the eight equivalent <111> directions.

Figure 11 shows the resonance of substitutional nitrogen in diamond for the external magnetic field parallel to the three principal directions in the crystal.

An isotropic g-value ($g = 2.0024 \pm 0.0005$) makes the position of the central resonance line (corresponding to the nuclear spin quantum number $m_I = 0$) independent of the orientation of the external magnetic field.

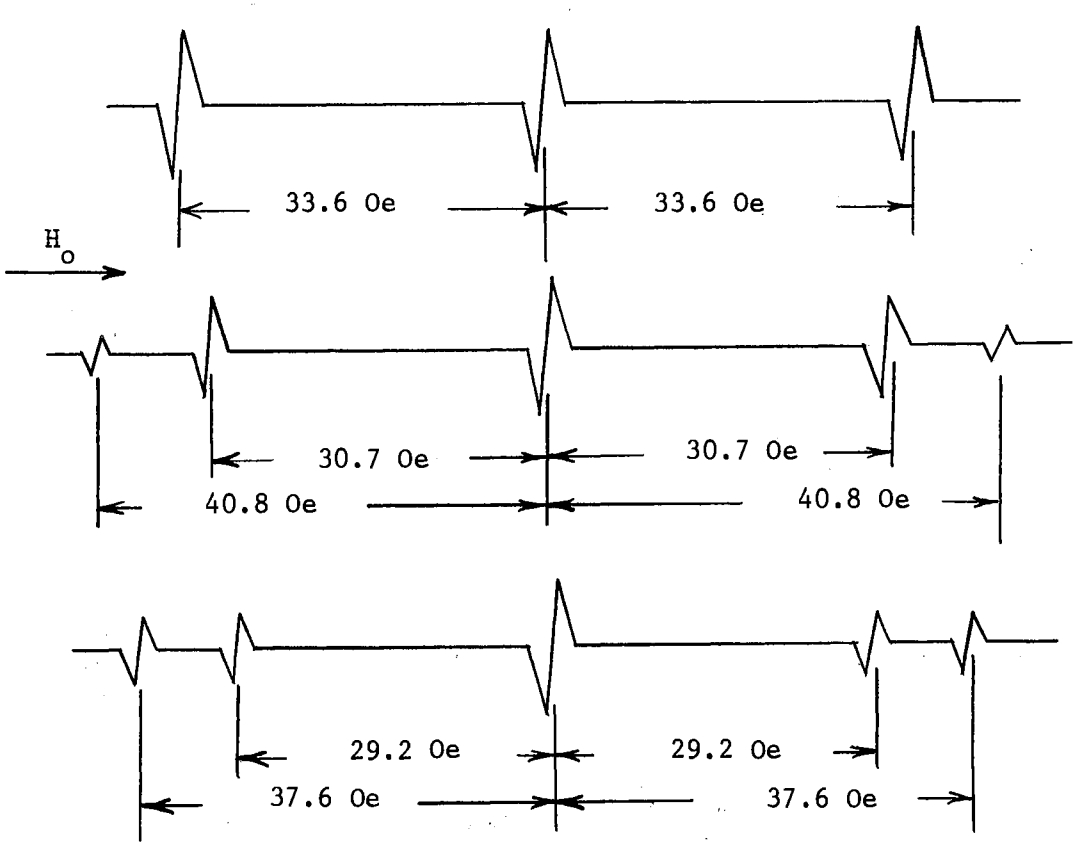

Figure 11. Schematic Representation of the ESR Spectrum of Substitutional Nitrogen Donors in Diamond

Since the electron is localized along the <111> directions, and the nuclear spin of nitrogen is 1, then the spectrum should consist of (2I + I) or three hyperfine resonance lines. However, the eight possible orientations of the orbital directions introduce the additional structure to the spectrum. Since reflection symmetry cannot be detected using ESR, the number of distinguishable sites is reduced to four. When the external magnetic field is parallel to a <100> direction, the bond directions all make an angle of 54^{o} 40' with $\vec{H}_o$. The electron sites are equivalent (that is, the component of the magnetic field along the bond directions is the same for every site); hence, the spectrum consists of 3 equally intense lines as shown in Figure 11. When $\vec{H}_o$ is parallel to

one of the <111> directions of the crystal, one-fourth of the bonds are parallel to the external field, and three-fourths of the bonds make an angle of 70.5° with $\vec{H}_o$. The ratio of the intensity of the components of the hyperfine lines corresponding to the nuclear quantum numbers $m_I = +1$ and -1 is 3-to-1 as shown in Figure 11. With $\vec{H}_o$ parallel to a <110> direction, one-half of the bond makes an angle of 35° 20' with $\vec{H}_o$, and one-half of the bonds are perpendicular to $\vec{H}_o$; hence, the ratio of 2-to-2 for the components of the outer hyperfine lines. For an arbitrary orientation each of the four sites distinguishable by ESR experiments "sees" a different component of the external field; hence, the outer lines can split into as many as four components.

Klingsporn, Bell and Leivo (36) reported a spectrum of a new nitrogen defect center in which the g and A tensors each has one of its principal components g_1 and A_1 oriented in a <110> direction. The orientation of the magnetic axis with respect to the principal axes of the host diamond crystal for one of the possible orientations of the center is shown in Figure 12.

However, this center has its g_1 and A_1 components randomly distribute among all the <110> directions. The g_2 component makes an angle $\psi = 45.2^{\circ}$ with the $[\bar{1}10]$ axis, and the A_2 component makes an angle $\alpha = 22.4$ with the $[\bar{1}10]$ for the center shown in Figure 12. Treating the center as having a T_d site symmetry, the number of equivalent orientations is 24. However, since ESR experiments cannot distinguish reflection symmetry, the number of distinguishable orientations is 12. This is true since the spin Hamiltonian is invariant under reflection. For $\vec{H}_o$ in a {110} plane, this center's hyperfine components should split into as many as seven distinct lines, five of which are of double in-

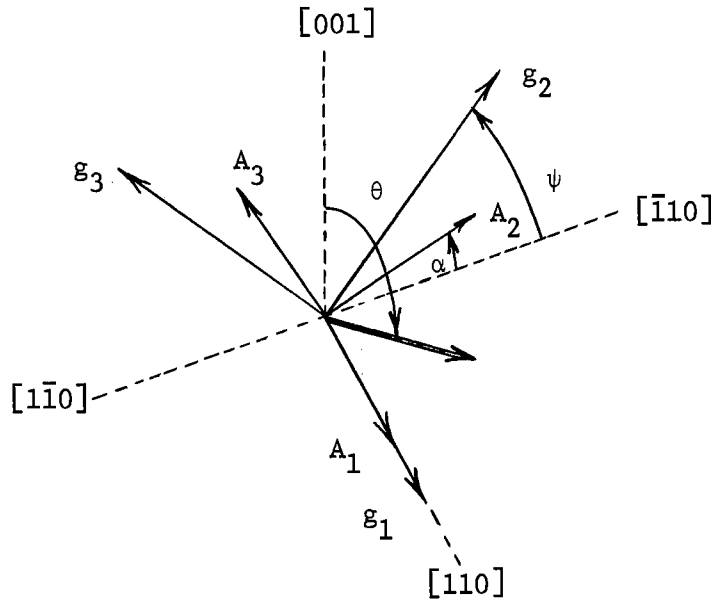

Figure 12. A Possible Defect Orientation Which Has its Principal Components g_1 and A_1 in the <110> Direction (after Klingsporn, et. al.).

tensity. The magnetic field strengths and relative intensities of the components of the hyperfine splittings with the field $\vec{H}_o$ parallel to the three principal directions in a {110} plane is shown in Figure 13. Along the principal directions some of the components of the hyperfine lines overlap, so that there is not the maximum of seven componetns for either the low, middle or high field hyperfine lines.

The orientation dependence of a center thought to be due to ionized nitrogen pairs in smoky-brown colored single crystal diamonds has been reported (65). The unpaired electron was assumed to be localized in an antibonding orbital along the N-C bond direction and weakly interacting with the second nitrogen atom. The principal directions of the hyperfine tensors are assumed to be parallel to the <111> directions. The g-value of the ionized nitrogen center is isotropic and reported to be 2.0024,

which is very close to the g-value of the center under investigation in this study.

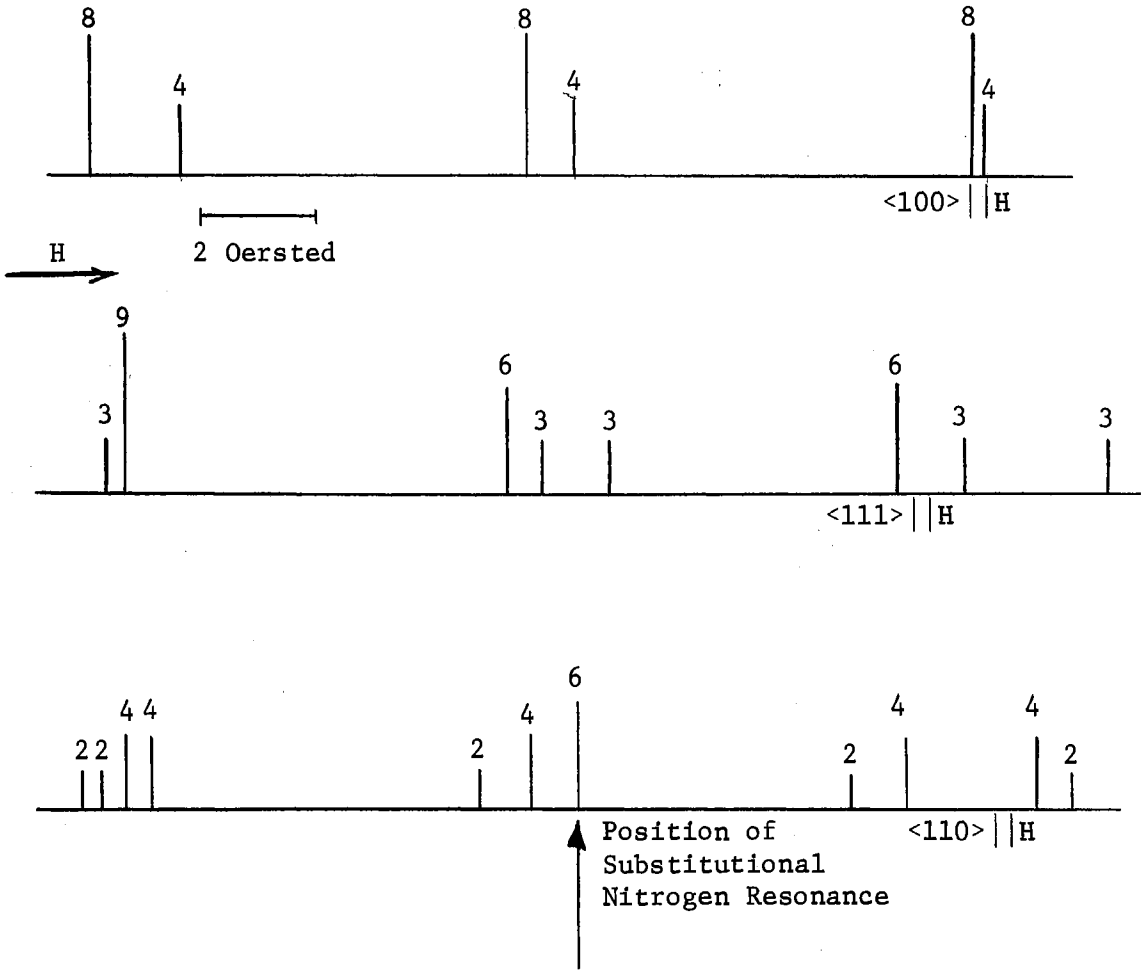

Figure 13. Hyperfine Structure With External Magnetic Field Parallel to the Principal Directions

The lines with the external field parallel to the principal directions is reproduced in Figure 14. The dotted lines correspond to the hyperfine lines of substitutional nitrogen. The arrows indicate the

approximate location of the hyperfine resonance lines of the center which is the object of this study.

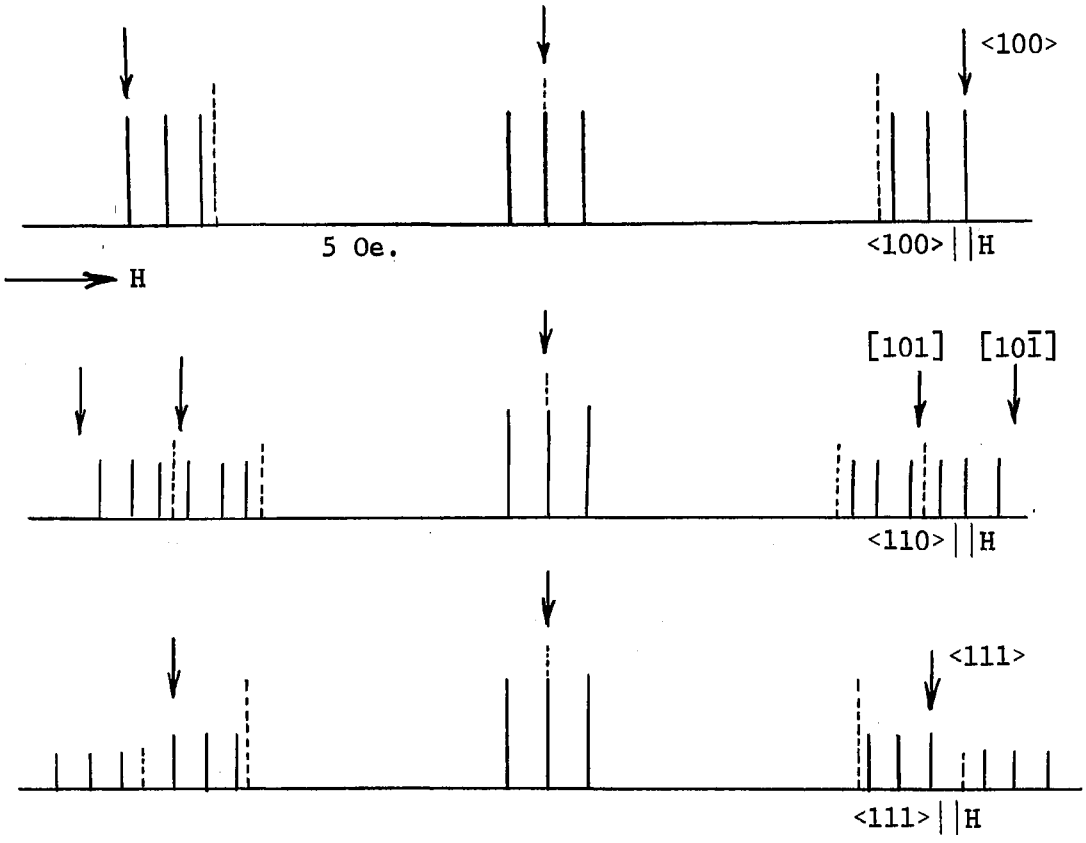

Figure 14. The Hyperfine Resonance Lines of Ionized Nitrogen Pairs (after Shcherbskova, et. al.)

Experimental Observations and Measurements

ESR Spectrum Observed in D-61

The ESR spectrum of samples D-60 and D-61 were identical. The

samples both exhibited the resonance of substitutional nitrogen defect centers. They also exhibited the complex resonance in the neighborhood of g = 2.0 as seen in Figure 15. Figure 15 shows the spectrum of D-61 with $\vec{H}$ parallel to the principal directions contained in the (010) plane. The magnetic field splitting of the outer hyperfine lines is shown in this figure. These are the hyperfine lines for $\Delta m_I = \pm 1$ for the center whose orientation dependence is the object of this study.

In order to determine if there were any hyperfine lines which were associated with this new center and which might have been masked by the complex spectrum, the sample was irradiated with UV light of wavelength of 366 mμ or 313 mμ. The UV irradiation caused an increase in the intensity of the ESR signal as shown in Figure 16.

It is known from an earlier study undertaken in this laboratory that the UV irradiation does not affect any of the components of the complex ESR signal (66). However, in this sample it is seen that there is an increase in one of the peaks in the complex ESR spectrum. The increase corresponds in intensity to the increase of the outer hyperfine lines. It was concluded, therefore, that there are three hyperfine lines associated with this new center. This would correspond to a nuclear spin of I = 1, since the number of hyperfine lines is given by (2I + 1).

Other than nitrogen, only H_2, Li, Cu^{64} and Cs^{130} have a nuclear spin of one. Both Cu^{64} and Cs^{130} are radioactive and have half-lives of only 12.8 hrs. and 30 min. respectively. Therefore, they are ruled out. Lithium has not been found in natural diamonds (67). This does not rule out lithium, but its presence is not nearly so attractive as that of nitrogen, which is common to all type I diamonds. Using a gas

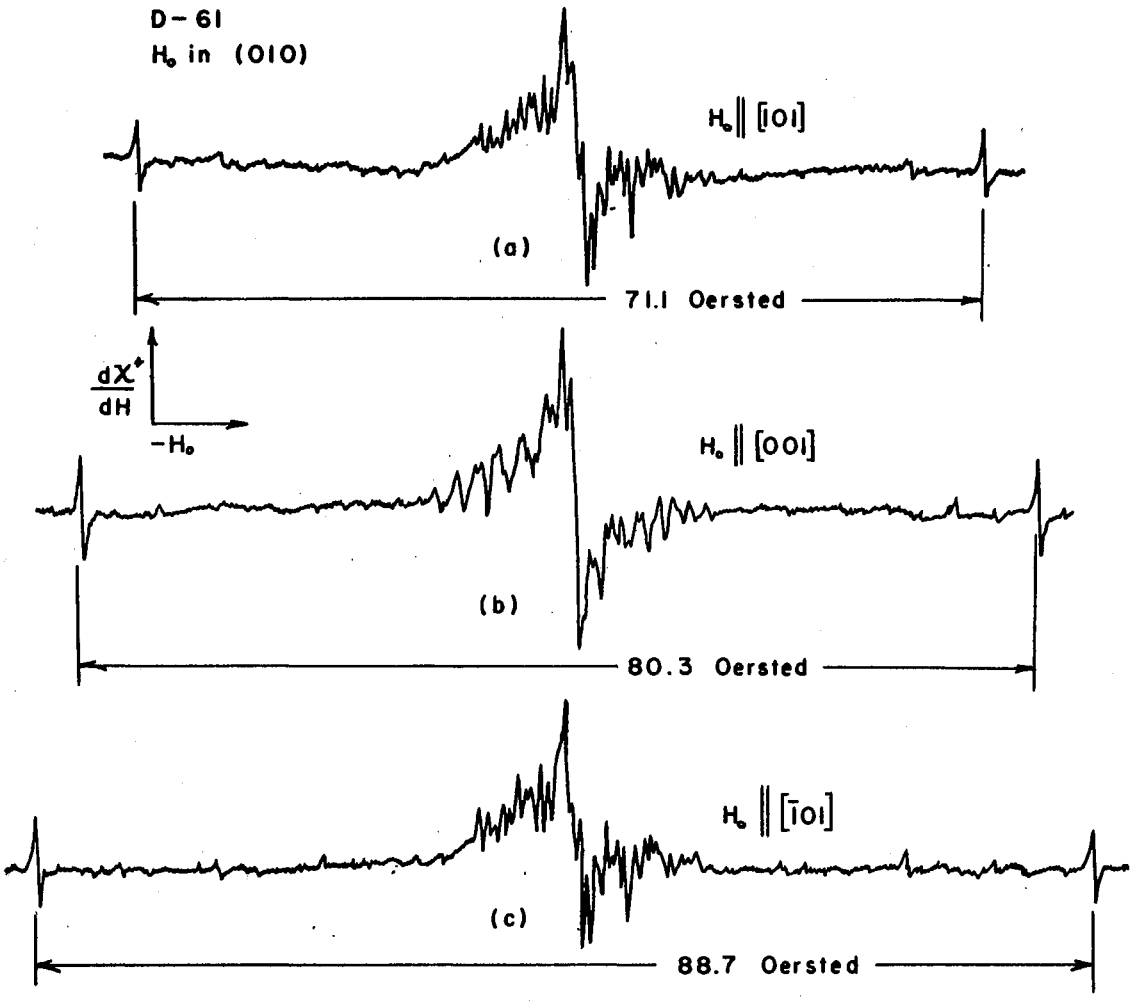

Figure 15. Electron Spin Resonance in Diamond D-61 With the Principal Directions in the (010) Plane Parallel to the Magnetic Field H_o

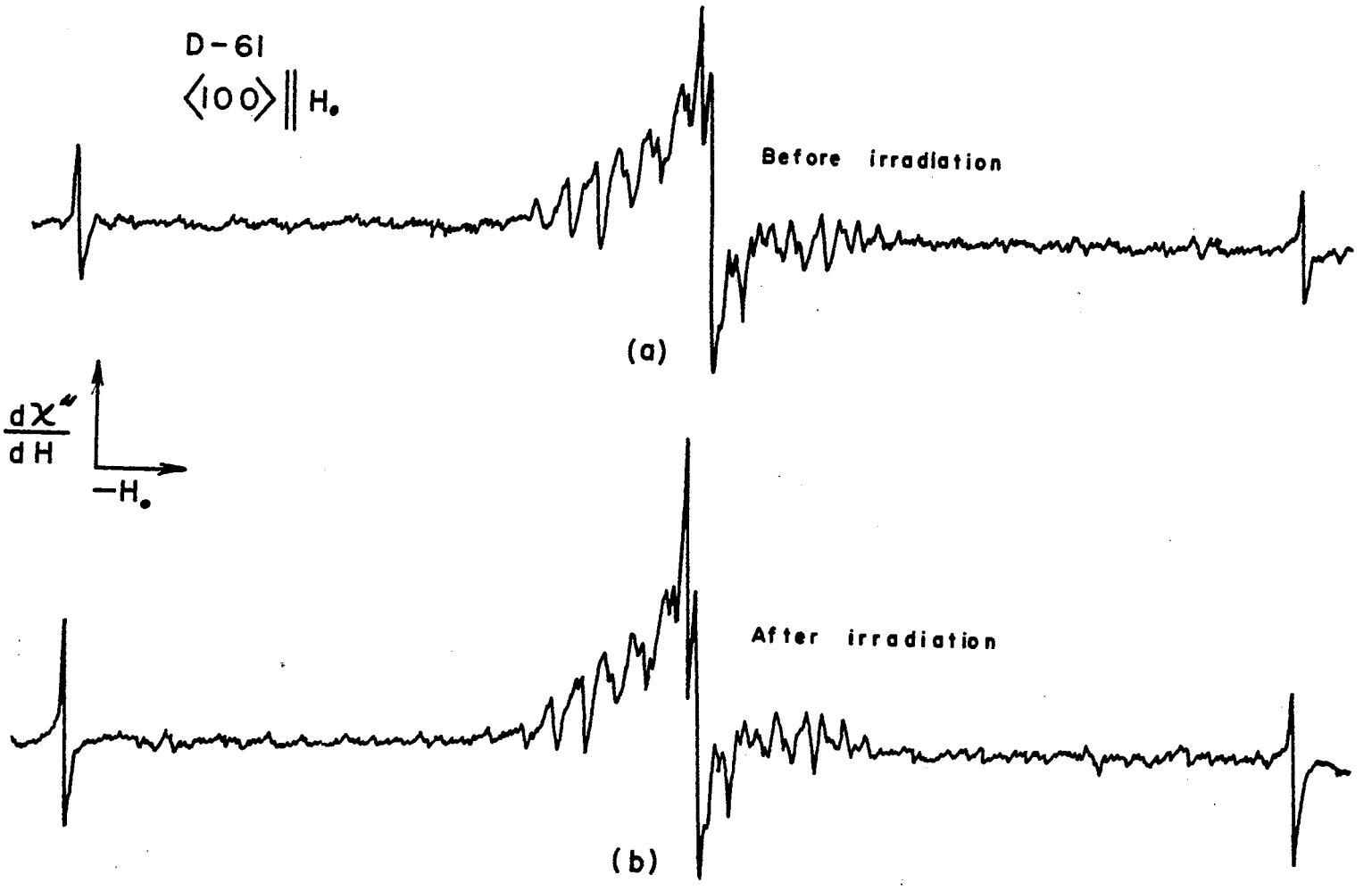

Figure 16. Effect of 313 mμ Irradiation on ESR Spectrum of Diamond D-61

analysis technique, Kaiser and Bond (23) found only small quantities of hydrogen in natural diamond. The spin one isotope of hydrogen can be ruled out since it has a natural abundance of only 0.015%. This leaves nitrogen the most promising choice since it is found in large concentrations in all type I natural diamonds.

It should be noted that in Figures 15 and 16 the hyperfine lines due to substitutional nitrogen are not present. The spectra shown in these two figures were taken with the modulation coils on the sample cavity in phase with the reference signal in the Varian 100 kc phase detection unit. The substitutional nitrogen resonance is maximized when the modulation coils on the sample cavity are driven 90° out of phase with respect to the reference signal. When the sample is run in phase, the substitutional nitrogen resonance intensity is zero. Since the reference phase can be adjusted continuously from 0° to 90° out of phase, the phase was set for 45° out of phase so that both the substitutional nitrogen resonance lines and the new nitrogen resonance lines were present. The runs at 45° out of phase with $\vec{H}_o$ parallel to the [001] and [$\bar{1}$01] axes are shown in Figure 17.

The spectra with $\vec{H}_o$ parallel to the [111] and the [$\bar{1}$01] axes are shown in Figure 18. These two spectra were run in phase; hence, the substitutional nitrogen resonance is not present, but the arrows indicate the location of the outer hyperfine peaks for substitutional nitrogen.

Orientation Behavior of the New Nitrogen Center

The intensity of the new nitrogen resonance dropped to zero whenever the magnetic field $\vec{H}_o$ was rotated 15° out of either the ($\bar{1}$01) plane

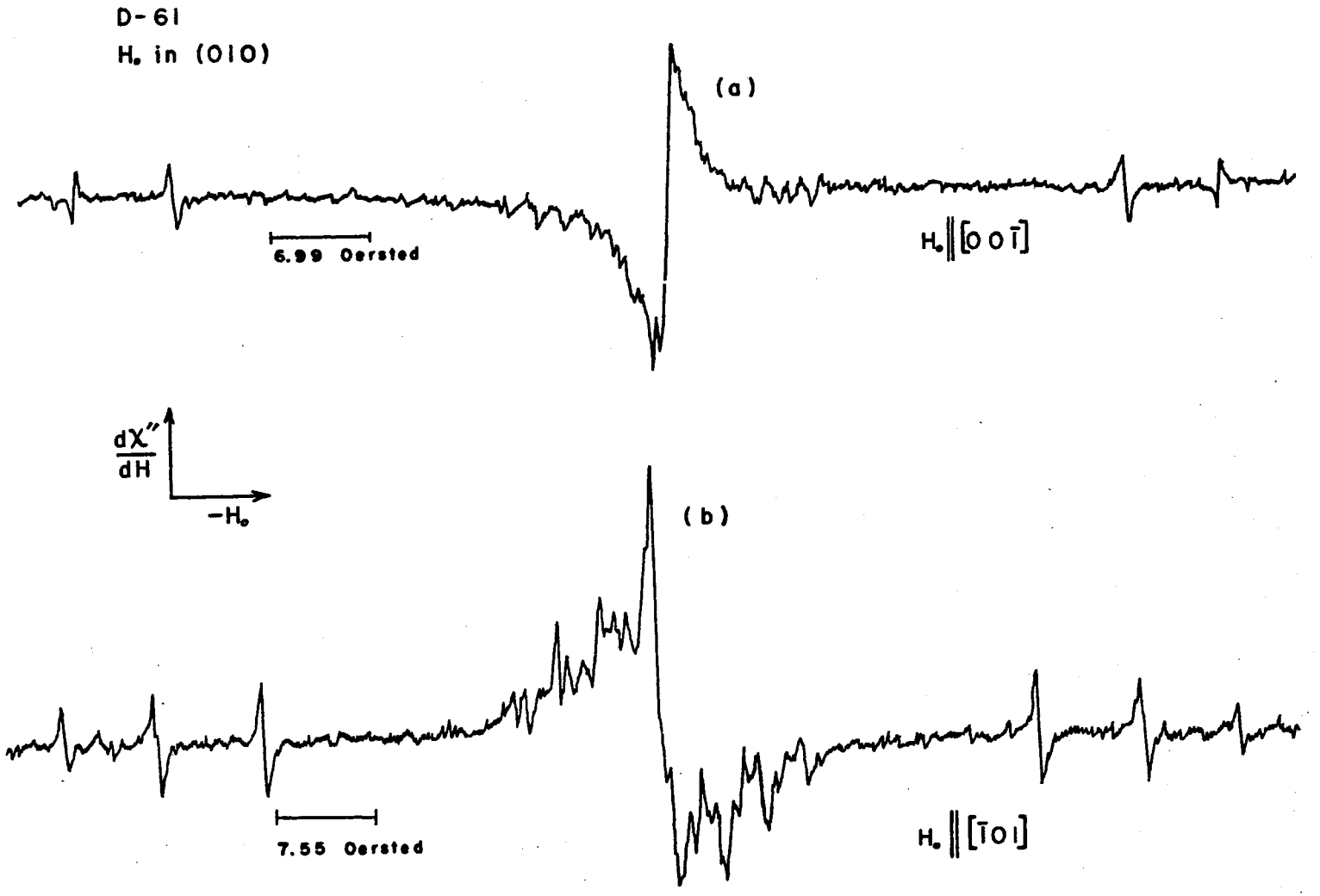

Figure 17. The ESR Spectra With the Reference Phase 45° Out of Phase

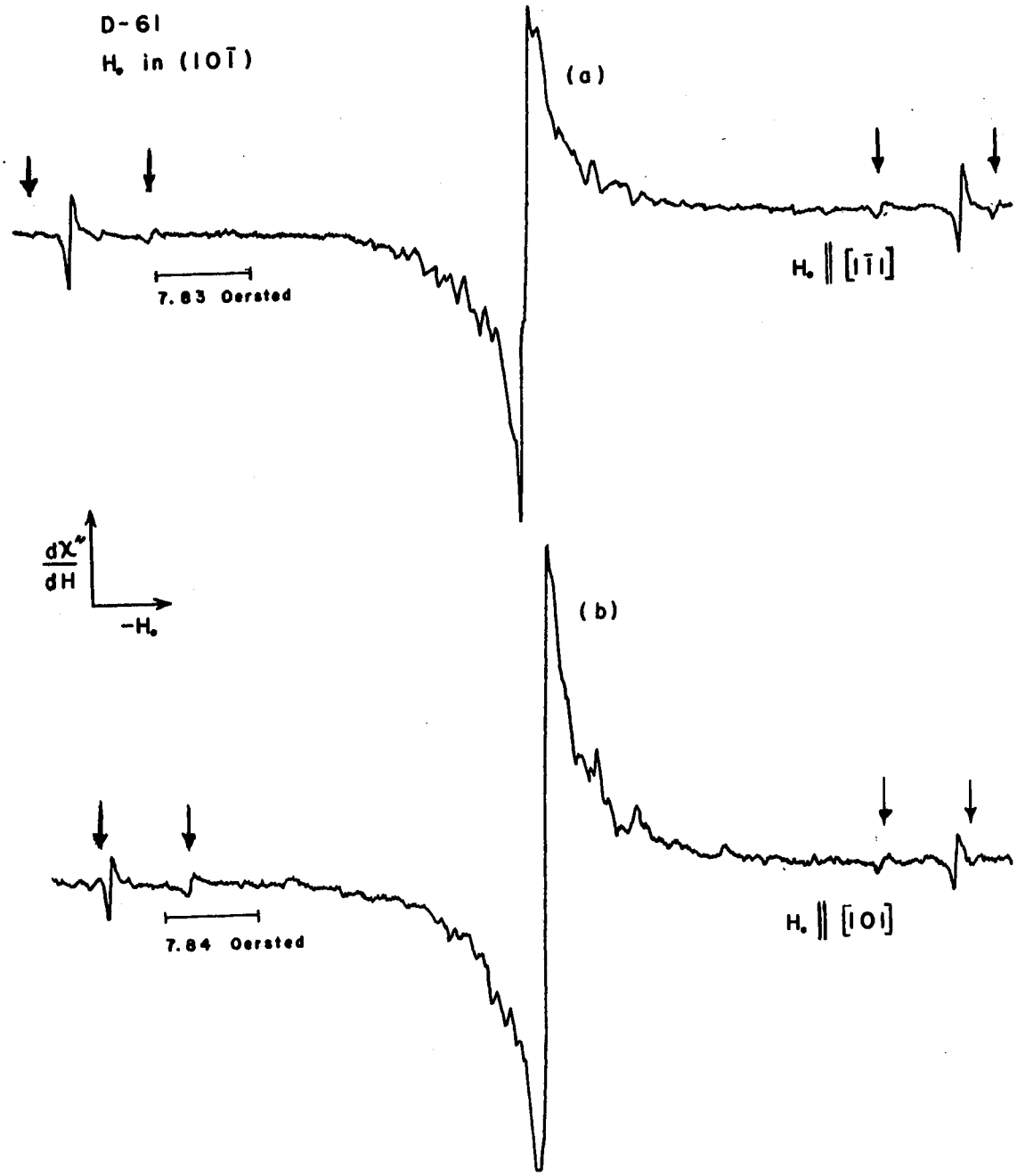

Figure 18. The ESR Spectrum in Diamond D-61

or the (010) plane. Therefore, the signal was observable only in 7 of the 13 principal directions. The splitting of the outer hyperfine lines and their approximate relative intensity is given in Table I.

TABLE I

DATA FOR OUTER HYPERFINE LINES IN DIAMOND D-61 WITH THE PRINCIPAL AXES PARALLEL TO THE MAGNETIC FIELD

Axis//$\vec{H}$	Exp. Splitting (Oe)	Theo Splitting (Oe)	Relative Intensity
$[10\bar{1}]$	88.7	88.7	10
[101]	71.7	71.7	6
[010]	81.6	81.5	10
[100]	80.0	80.4	10
[001]	80.4	80.4	10
$[1\bar{1}1]$	74.2	74.7	8
$[\bar{1}1\bar{1}]$	74.8	74.7	8

The theoretical calculations of the splitting given in Table I will be explained later.

Several interesting observations about the data in Table I should be pointed out. As stated earlier, the intensity of the resonance is observable only in the (010) and the $(\bar{1}01)$ planes. The largest hyperfine splitting is observed with $\vec{H}_o$//$[\bar{1}01]$ axis, which is perpendicular to the $(\bar{1}01)$ plane. The smallest splitting is with $\vec{H}_o$//[101], which is the axis formed by the intersection of the (010) and $(\bar{1}01)$ planes. Also, the splitting with $\vec{H}_o$//[010] was found to be approximately one oersted greater than with $\vec{H}_o$//[100] and $\vec{H}_o$//[001]. As will be seen later, this is predicted by theory. However, the difference in splitting with $\vec{H}_o$//$[1\bar{1}1]$ and $\vec{H}_o$//$[\bar{1}1\bar{1}]$ is most likely due to experimental error.

At this point the procedures for taking data and estimates of experimental error should be discussed. As outlined in Chapter III, the scan rate was measured using an NMR probe. Over one scan or run (the approximate range of a scan or run being from a field strength of 3200 oersted to one of 3300 oersted) the NMR oscillator was continually readjusted so that the external field scanned through the NMR resonance about twelve times. The NMR frequency versus chart displacement was plotted to obtain the scan rate. For each run this plot was done using a linear least square fit with the aid of the IBM-360 computer. Magnetic field strengths were calculated for as many as ten runs with the same orientation and it was found that the field strengths calculated seldom varied more than 0.1 oersted.

In order to calculate the magnetic field strength a standard sample with a known g-value must be placed in the sample cavity. The magnetic field at the chart displacement where the standards resonance occurs can then be calculated. The standard generally used is DPPH whose g-value is known accurately. However, because of the large complex signal in the neighborhood of $g = 2.0$ DPPH could not be conveniently used because the intensity of both sample's resonances with both samples in the cavity caused the chart recorder to go off scale. Therefore, for a reference point the substitutional nitrogen resonance was used since its g-value of 2.0027 ± 0.0005 is known from literature (25).

The orientation of the sample in the cavity also introduced error. An error of as much as one-half an oersted was observed for principal directions where the resonance lines were most highly field orientation dependent. For each principal direction at least 10 runs were made and an average taken to obtain the field strength for each resonance line.

The experimentally observed angular dependence of the new nitrogen resonance is shown in Figures 19 through 24. The experimentally measured data points are shown as circles. The solid lines correspond to the theoretically calculated angular dependence and will be discussed in detail in the next section.

Figures 19 and 20 dislplay the angular dependence as $\vec{H}_o$ is rotated in the $(\bar{1}01)$ and (010) planes respectively, which are the two planes in which the intensity of the ESR spectrum is always observable. For all these figures the magnetic field strength is plotted against the angular rotation of the field for the low, middle, and high field hyperfine components. Figures 21 and 22 display the angular dependence as $\vec{H}_o$ is rotated in the (100) and (001) planes respectively. The inequivalence of these two orientations and the angular dependence when $\vec{H}_o$ is rotated in the (010) plane is very evident. Figure 23 shows the angular dependence with $\vec{H}_o$ rotated in the (110) plane and Figure 24 shows the angular dependence with $\vec{H}_o$ rotated in the $(1\bar{1}\bar{1})$ plane.

Optical Data

The infrared absorption of diamonds D-60 and D-61 are almost identical, as is the infrared absorption of several of the diamonds with the complex structure in the neighborhood of g = 2.0. All the diamonds with the complex structure exhibit a strong absorption peak at 7.3μ (53).

Optical absorption data in the visible and ultraviolet region of the electromagnetic spectrum were taken for diamonds D-60, D-61, and D-18. Diamond D-18 is a clear white diamond with the complex ESR spectrum, but it does not have the ESR spectrum whose orientation dependence is the object of this study. All the specimens exhibit a sharp absorp-

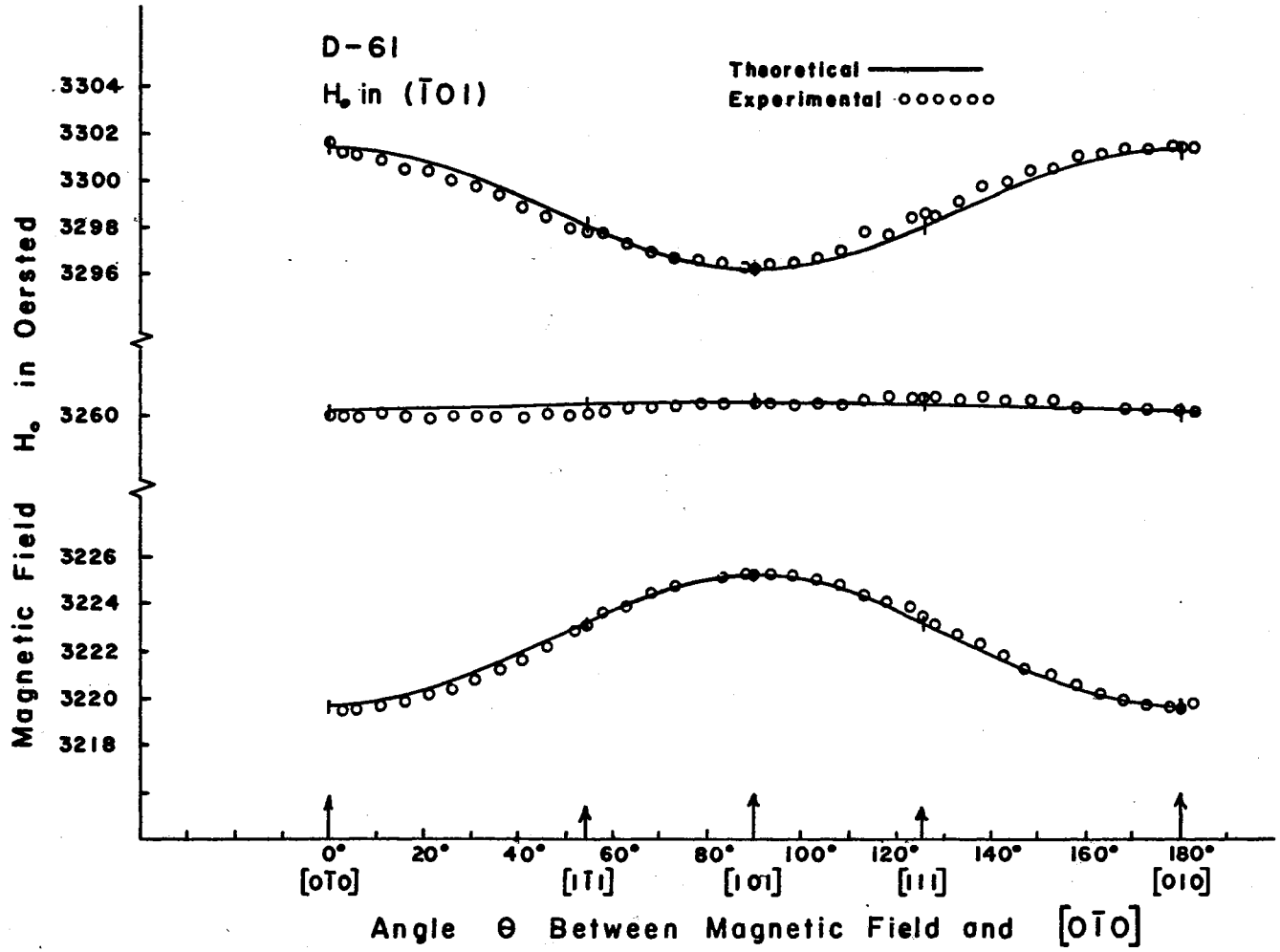

Figure 19. Experimental and Theoretical Angular Dependence of the Three Hyperfine Components With $\vec{H}_o$ Rotated in the ($\bar{1}01$) Plane

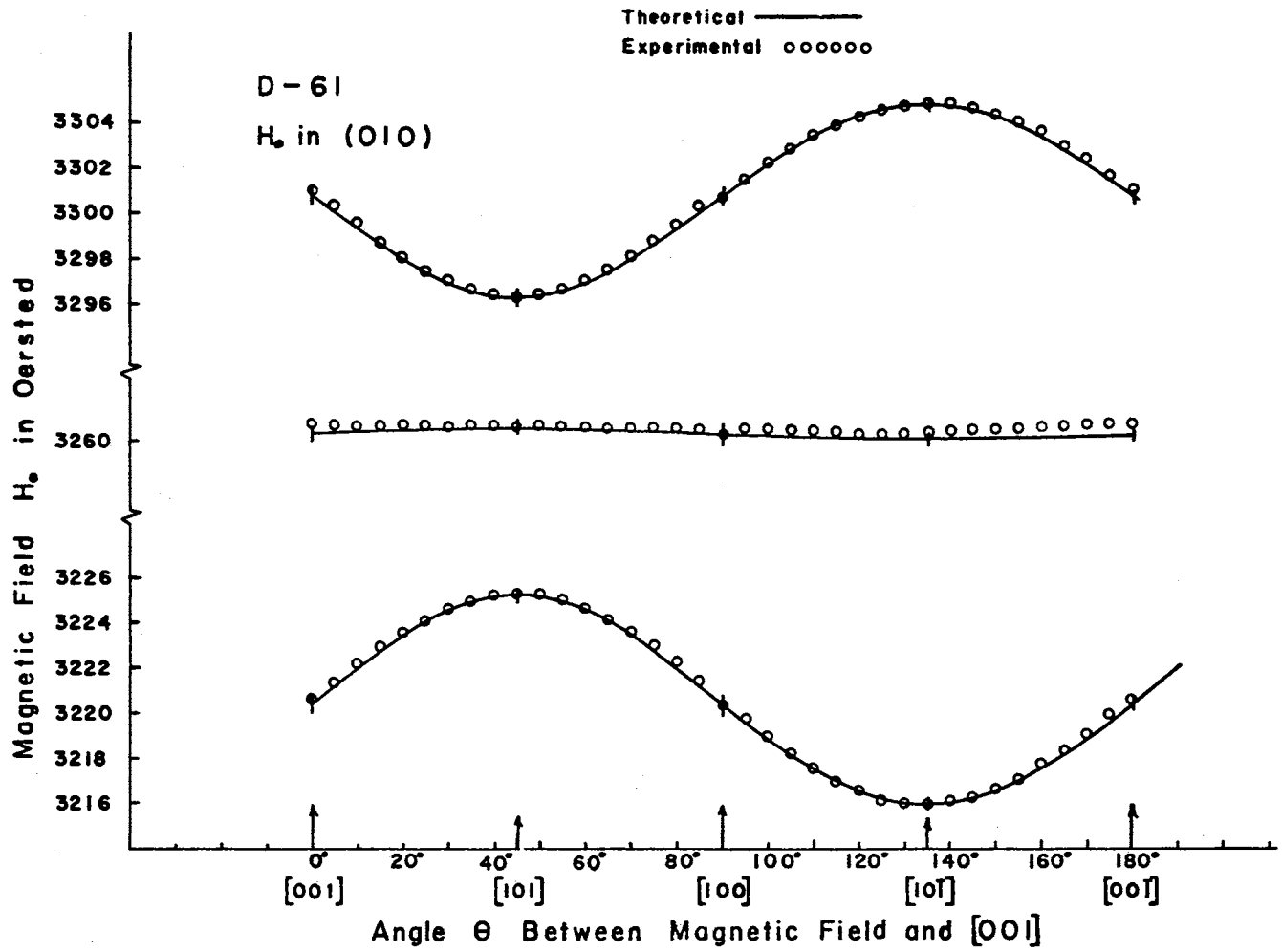

Figure 20. Experimental and Theoretical Angular Dependence of the Three Hyperfine Components With $\vec{H}_o$ Rotated in the (010) Plane

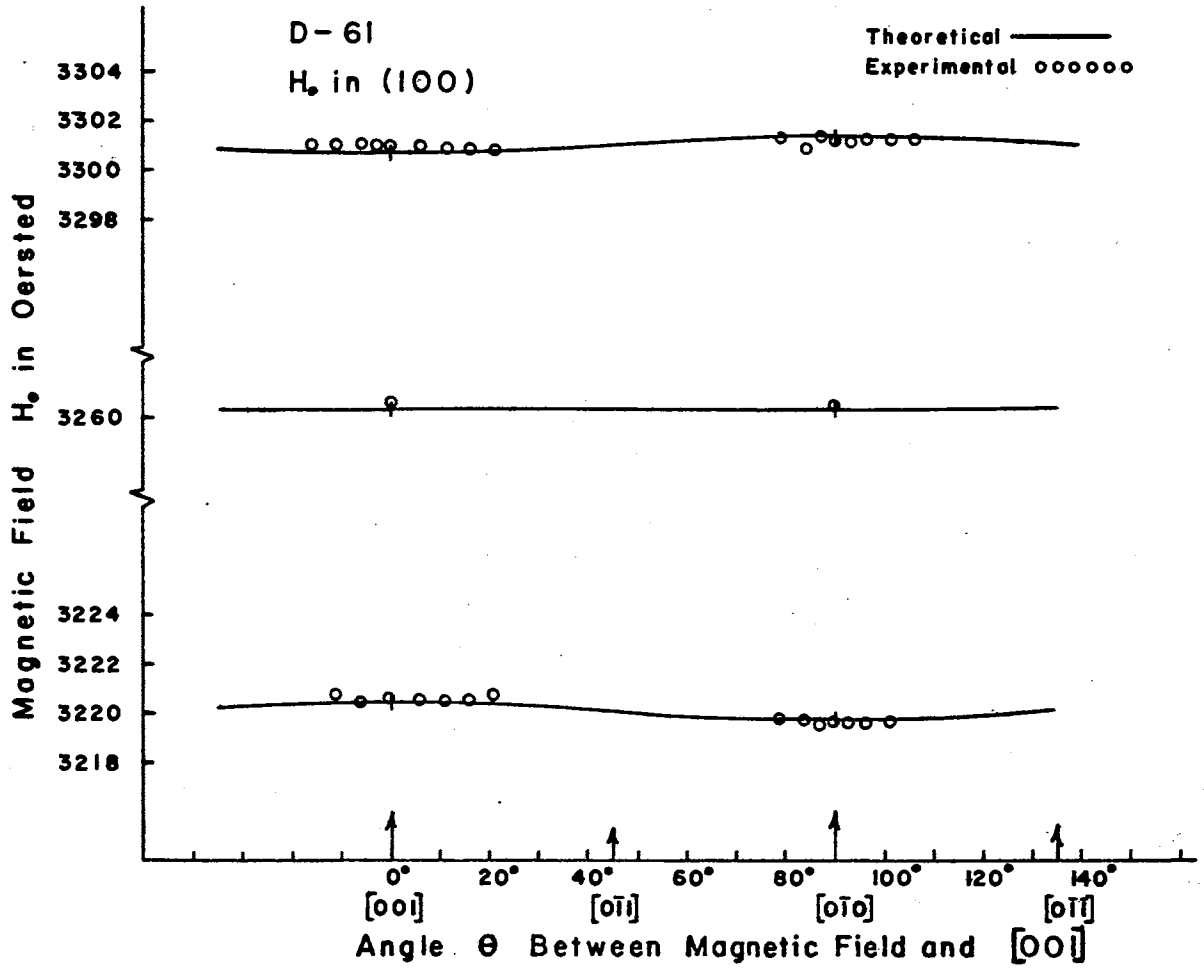

Figure 21. Experimental and Theoretical Angular Dependence of the Three Hyperfine Components With $\vec{H}_o$ Rotated in the (100) Plane

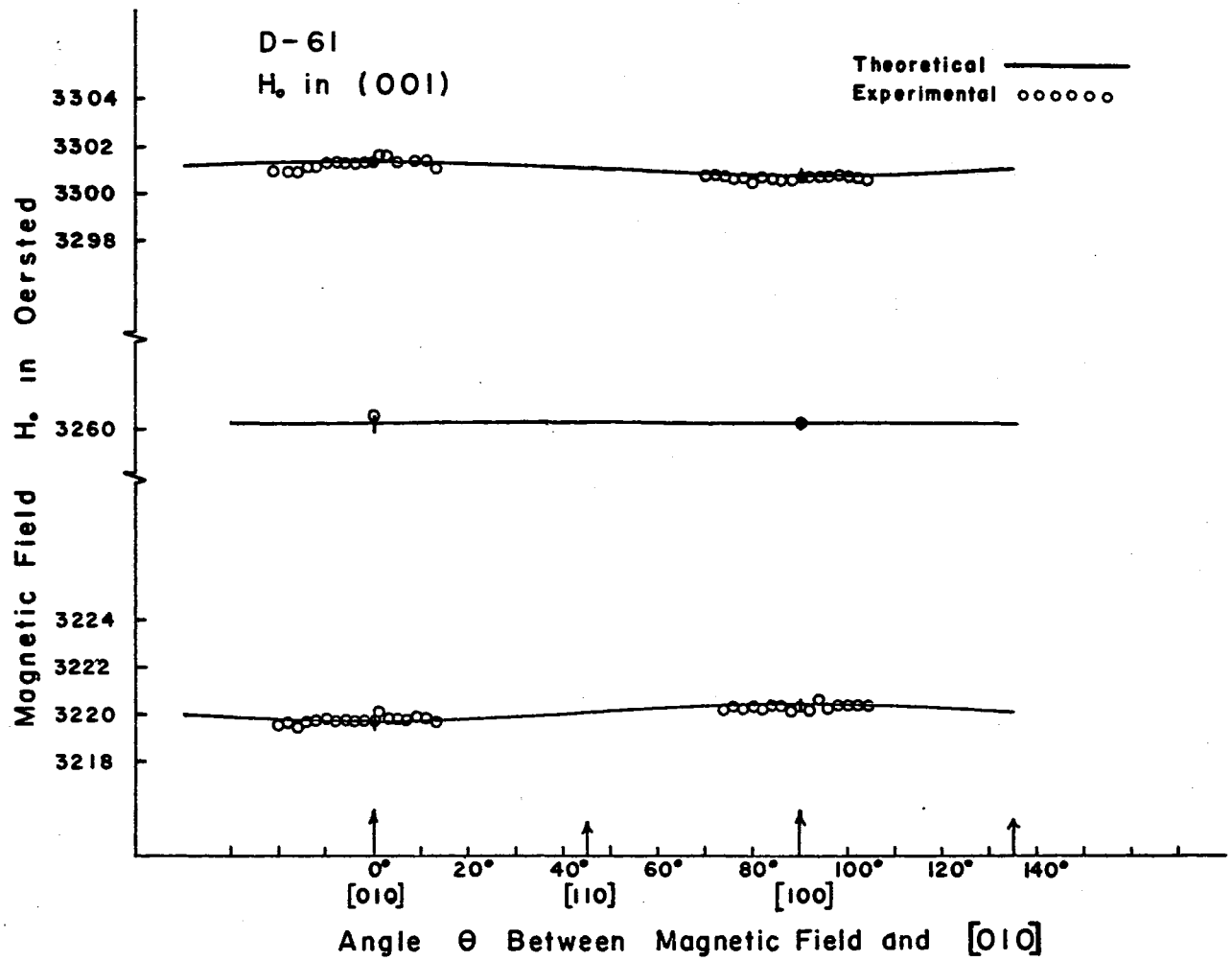

Figure 22. Experimental and Theoretical Angular Dependence of the Three Hyperfine Components With $\vec{H}_o$ Rotated in the (001) Plane

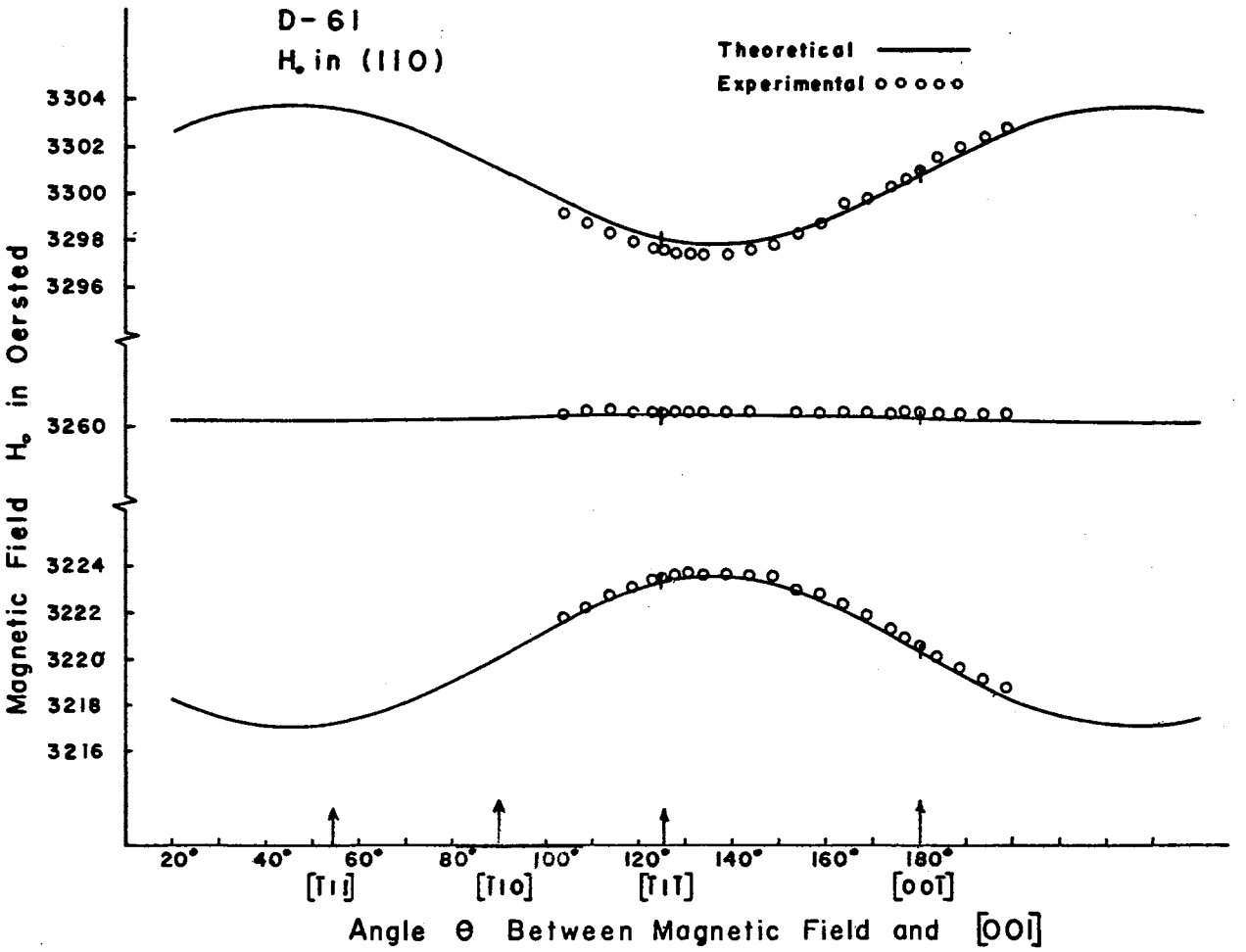

Figure 23. Experimental and Theoretical Angular Dependence of the Three Hyperfine Components With $\vec{H}_o$ Rotated in the (110) Plane

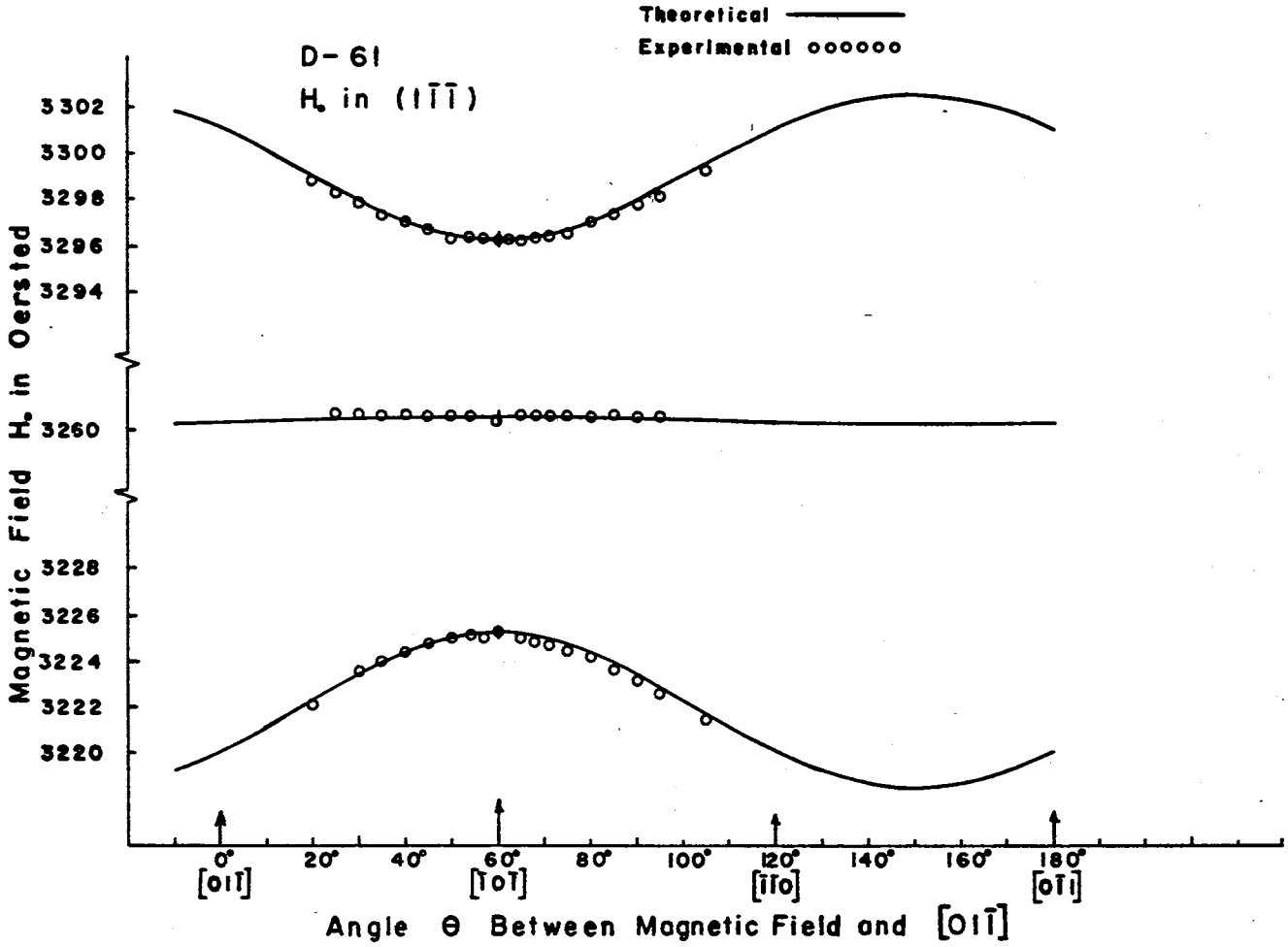

Figure 24. Experimental and Theoretical Angular Dependence of the Three Hyperfine Components With $\vec{H}_o$ Rotated in the (1$\bar{1}\bar{1}$) Plane

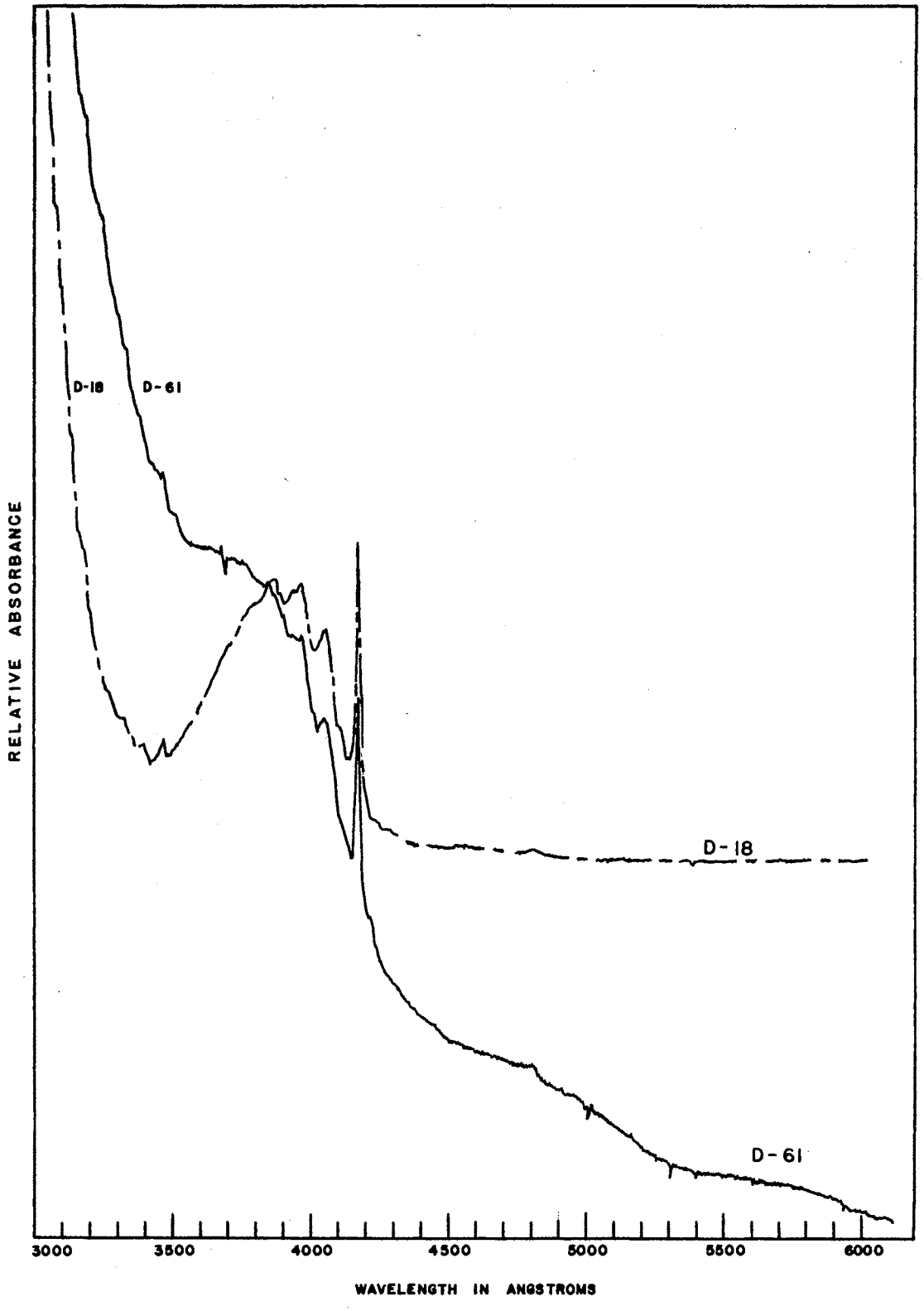

Figure 25. Optical Absorption of Diamonds D-61 and D-18 in the Visible and the Ultraviolet Regions

tion peak at 4150 A (2.98 eV) and a sharp cut-off in the ultraviolet in the neighborhood of 3000 A. Figure 25 shows the absorption spectrum for diamonds D-61 and D-18 at room temperature. However, no prominent features in the optical absorption spectra are present which would distinguish D-60 or D-61 from those diamonds in our collection in which the new ESR spectrum is unobservable.

The Spin Hamiltonian and Calculations

As stated earlier, it is believed that a nitrogen nucleus of spin one is responsible for the three hyperfine resonance lines observed in the unusual ESR spectrum observed in samples D-60 and D-61.

The spin Hamiltonian characterizing the Zeeman and hyperfine interactions which have been assumed to be present will be of the form

$$H = \beta \vec{H} \cdot \underline{g} \cdot \vec{S} + \vec{I} \cdot \underline{A} \cdot \vec{S}, \qquad (4\text{-}1)$$

where $S = \frac{1}{2}$ and $I = 1$. The magnitude of the principal components of the g and A tensors and their principal axes must be determined in order to describe the resonance spectrum.

The Breit-Rabi expression for the energy levels of the Hamiltonian given by Equation (4-1) for the allowed ESR transitions $\Delta m_s = \pm 1$ and $\Delta m_I = 0$ are

$$h\nu = g\beta H + m_I A + \frac{A^2}{2g\beta H}\left[I(I+1) - m_I^2\right], \qquad (4\text{-}2a)$$

where

$$g^2 = g_1^2 \cos^2 \phi_1 + g_2^2 \cos^2 \phi_2 + g_3^2 \cos^2 \phi_3, \qquad (4\text{-}2b)$$

and

$$A^2 = A_1^2 \cos^2 \Phi_1 + A_2^2 \cos^2 \Phi_2 + A_3^2 \cos^2 \Phi_3. \qquad (4\text{-}2c)$$

The angles ϕ_i and Φ_i are the angles between the principal axes of the g and A tensors, respectively, and the external magnetic field $\vec{H}_o$.

In order to plot the angular dependence of the different hyperfine components, Equation (4-2a) was solved explicitely in terms of the magnetic field, yielding

$$H = \frac{1}{2g\beta}\left[h\nu - m_I A + \sqrt{(h\nu - m_I A)^2 - 2A[I(I+1) - m_I^2]}\right] \qquad (4\text{-}3)$$

The fact that the hyperfine lines never split into components indicates that the center is not distributed evenly among the different equivalent sites of the host crystal. Since the $(10\bar{1})$ and (010) planes are perpendicular and because of the symmetry of the spectrum about the $[\bar{1}01]$, [010] and [101] which are orthogonal, these axes were initially chosen as the principal axes system for both the g and A tensor. It should be noted here that in the ESR spectrum none of the additional possible orientations can be distinguished from the orientation from which it was obtained by a 180^o rotation. In other words, the spin Hamiltonian is invariant to reflection.

The anisotropic features of the spectrum can be explained on the basis of a model in which the defect center is oriented so that both the g and A tensor's principal axes are coincident and lie along the $[\bar{1}01]$, [010] and [101] axes of the host diamond crystal as shown in Figure 26.

The effective value of g given by Equation (4-2b) must be calculated in terms of the principal axes chosen for $\underline{g}$ and $\underline{A}$. The angular dependence of the effective values of g and A for a defect center with one component of g and A oriented along a <110> axis is given in literature (68). If $\vec{H}_o$ is rotated in the $(\bar{1}01)$ plane and measuring θ from the [001] axis, the effective g-value is given by

$$g = \{g_2^2 \sin\theta + g_3^2 \cos^2\theta\}^{\frac{1}{2}}. \qquad (4\text{-}4)$$

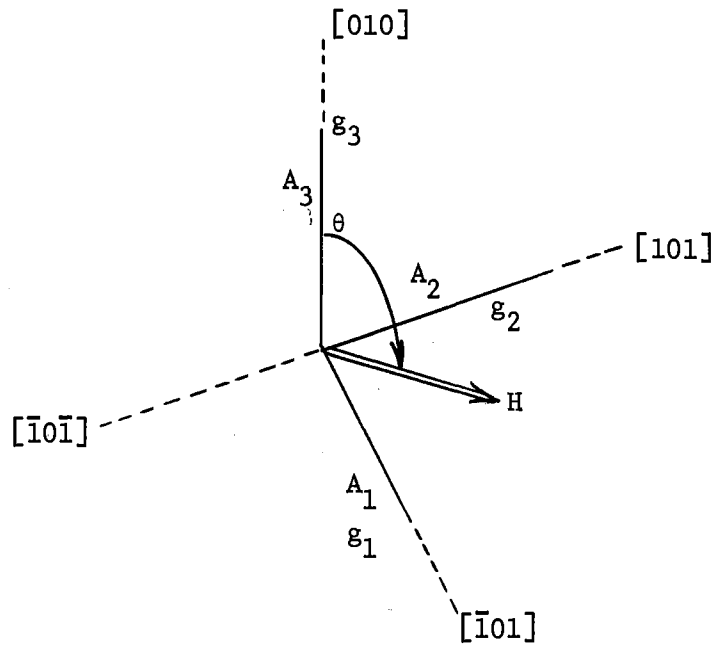

Figure 26. Defect Orientation for the Principal Axes of the g and A Tensors

The expression for the effective value for A is identical in analytic form to that of g. With $\vec{H}_o$ in the (010) plane the effective g-value is given by

$$g = \{g_1^2 \cos^2(45^\circ + \theta) + g_2^2 \sin^2(45^\circ + \theta)\}^{\frac{1}{2}}, \qquad (4\text{-}5)$$

where θ is measured from the [001] axis. With $\vec{H}_o$ in the (100) plane the effective g-value is given by

$$g = \{\tfrac{1}{2} g_1^2 \sin^2\theta + \tfrac{1}{2} g_2^2 \cos^2\theta + g_3^2 \sin^2\theta\}^{\frac{1}{2}}, \qquad (4\text{-}6)$$

where θ is measured from the [001] axis. With $\vec{H}_o$ in the (001) plane the effective value of g is given by

$$g = \{\tfrac{1}{2} g_1^2 \cos^2\theta + \tfrac{1}{2} g_2^2 \cos^2\theta + g_3^2 \sin^2\theta\}^{\frac{1}{2}}, \qquad (4\text{-}7)$$

where θ is measured from the [100] axis. With $\vec{H}_o$ in the (110) the effective g-value is given by

$$g = \{g_1^2 [\frac{\cos\theta}{\sqrt{2}} - \frac{\sin\theta}{\sqrt{2}}]^2 + \tfrac{1}{4} g_2^2 [-\sin\theta + \sqrt{2}\cos\theta]^2 + \tfrac{1}{2} g_3^2 \sin^2\theta\}^{\frac{1}{2}}. \qquad (4\text{-}8)$$

With $\vec{H}_o$ in the $(1\bar{1}\bar{1})$ plane the effective value of g is given by

$$g = \{\tfrac{1}{4} g_1 [\frac{\sin\theta}{\sqrt{3}} - \cos\theta]^2 + g_2^3 [-\frac{3}{2\sqrt{3}}\sin\theta - \tfrac{1}{2}\cos\theta]^2 + g_3^2 [\frac{1}{\sqrt{6}}\sin\theta - \frac{1}{\sqrt{2}}\cos\theta]^2\}^{\frac{1}{2}}. \qquad (4\text{-}9)$$

Using Equation (4-3) and substituting in the effective values of g and A given by Equations (4-4) through (4-9) the magnetic field strength at which the hyperfine resonance lines should occur can be calculated as a function of the angular displacement θ. The theoretical angular dependence for these six orientations is shown as the solid lines in Figures 19 through 24.

Using the IBM-360 computer the parameters were adjusted to yield the best over-all correlation with the experimental data. The resulting parameters were:

$$g_1 = 2.0021 \pm 0.0005$$
$$g_2 = 2.0019 \pm 0.0005$$
$$g_3 = 2.0020 \pm 0.0005$$

and

$$A_1 = 4.149 \pm 0.005 \times 10^{-3} \text{ cm}^{-1}$$
$$A_2 = 3.323 \pm 0.005 \times 10^{-3} \text{ cm}^{-1}$$
$$A_3 = 3.811 \pm 0.005 \times 10^{-3} \text{ cm}^{-1}$$

The Breit-Rabi expression for the energy from which Equation (4-3) was obtained was derived by neglecting any anisotropy in g. The expression is acceptable for this analysis since the anisotropy of g is only 0.01% of the average magnitude of g. Furthermore, Equation (4-3) was obtained neglecting anisotropy in A for second-order terms. However, the average magnitude of A (3.7×10^{-3} cm^{-1}) is sufficiently small so that the second-order terms do not contribute significantly.

X-Ray Diffraction Observations

Anomalies in the Laue back-reflection patterns of diamond D-61 were observed. The back reflection spots in the pattern appear as streaks instead of a clearly defined spot. The streaks were very pronounced (some as long as one quarter of an inch on a 3 cm. sample to film distance) for some orientations and hardly noticable with other orientations. With the [010] axis parallel to the X-ray beam the streaks were very pronounced, but with the [100] parallel to the beam the streaks are barely ascertainable. They appear relatively strong when the [001] axis is parallel to the X-ray beam.

Streaks in the Laue pattern of a crystal are commonly caused by distortions of the crystal when impurities in the host crystal form into platelets. Nitrogen is known to form platelets in the cubic planes of the diamond crystal (29). However, if nitrogen platelets are responsible for the streaks observed in the Laue patterns, then the streak pat-

terns for equivalent directions such as the [100] directions should be similar. This not being the case, it is possible that the imperfections causing the streaks are preferentially oriented in the crystal. In light of the seeming preferential orientation of the defect center responsible for the unusual ESR spectrum in this sample, this assumption does not seem too unreasonable.

An attempt to anneal out the center causing either the X-ray diffraction streaks or the center giving rise to the new ESR signal was undertaken. The diamond was heated to approximately 1100^{o} C. at a pressure of approximately 2×10^{-6} mm. However, the annealing did not affect either the intensity of the streaks on the X-ray pattern nor the intensity of the ESR signal.

Discussion and Conclusions

The fact that the hyperfine lines never split into components indicates that the center is not distributed evenly among the different sites in the crystal that are equivalent to the magnetic axis $[\bar{1}01]$, [101] and [010]. For an unpaired electron associated with a single nitrogen atom such as reported by Klingsporn, et. al. (36), the T_d site symmetry of the defect center in the diamond lattice could give rise to 24 components of the ESR spectrum. Reflection symmetry reduces the distinguishable number of lines to 12 for an arbitrary orientation of the magnetic field. For $\vec{H}_o$ in a {110} plane a defect center with one of the principal components of g and A along any one of the <110> directions, the number of distinct lines should be reduced to seven, five of which are of double intensity. This is what was observed by Klingsporn (68).

The center which is the object of this study has one of the com-

ponents of g and A in a <110> direction, but there is only one distinguishable hyperfine line for each orientation of the nuclear moment.

The formation of this defect center in a preferred orientation must have resulted from some unusual circumstance in the environment in which the crystal was formed, such as a large pressure gradient along a particular axis of the crystal. This might also account for the anisotropy in the streaks of the Laue patterns. However, it is not yet known if the defect causing the streaks in the Laue pattern and the defect giving rise to the ESR spectrum are in anyway related.

Probably one of the most interesting observations about this center and the center thought to be due to ionized nitrogen pairs is that they both have approximately the same g-value (2.0024 for the ionized nitrogen pairs) and the position of the hyperfine lines for this center falls very close to one of the components of the ionized nitrogen pair spectrum when the external field is parallel to the principal directions of the crystal. The location of the hyperfine lines of this center relative to the hyperfine components of the ionized nitrogen pair is shown in Figure 14. The arrows indicate the approximate position of the hyperfine lines for the principal directions in which they are present.

If this center is a preferentially oriented ionized nitrogen pair, it would be consistent with the fact that upon irradiation with UV light the signal increases; whereas the substitutional nitrogen donor signal decreases upon being ionized by the UV irradiation.

If the relative intensity shown for the components of the hyperfine structure are to scale for the ionized nitrogen resonance, (the relative intensity of the substitutional nitrogen resonance reported in the original article were not drawn to scale) then the relative intensity of

this resonance with $\vec{H}_o$ parallel to the principal axes of the crystal corresponds to the intensities shown for the ionized nitrogen pairs, except for $\vec{H}_o$ parallel to the $[\bar{1}01]$ direction where the intensity of the signal measured is too large by a factor of 2.

Summary

The new ESR spectrum observed in the two natural type I diamonds consists of three anisotropic hyperfine lines. The fact that the hyperfine lines never split into components for an arbitrary orientation of the external magnetic field suggests that this defect center is preferentially oriented in the host diamond crystal. The three hyperfine lines further suggest that the spectrum arises from the hyperfine interaction of an unpaired electron with a spin-one nucleus. The most promising impurity with a spin-one nucleus was considered to be nitrogen.

The spin Hamiltonian charcterizing the defect center is of the form $H = \beta\vec{H}\cdot g\cdot\vec{S} + \vec{I}\cdot\underline{A}\cdot\vec{S}$ where $S = \frac{1}{2}$ and $I = 1$. Figures 19 through 24 show that number of lines and their angular behavior is predicted by a model in which the defect center has the principal components of both its g and A tensor coincident and parallel to the $[\bar{1}01]$, $[101]$, and $[010]$ axes. The angular dependencies shown in Figures 19 through 24 were calculated using the Breit-Rabi expression for the energies absorbed for the allowed ESR transitions and are in good agreement with the experimentally observed angular behavior.

Anomalies in the Laue back-reflection patterns where the back reflection spots appear as streaks were observed. Streaks or "spikes" in the Laue pattern are known to be caused by nitrogen platelets in diamonds. However, the inequivalence of the streak patterns along equiva-

lent directions of the host crystal suggests that the defects causing the streaks are also preferably oriented.

In order to determine if the defects causing the X-ray streaks and those causing the new ESR signal were related, the sample was heat treated to approximately 1100° C. and 2×10^{-6} mm. pressure. This treatment did not affect the intensity of either phenomenon. A more detailed annealing experiment at pressures of approximately 60 kilobars and 1150° C. to 1200° C. might prove to be of interest, since X-ray spikes due to nitrogen platelets have been annealed out under these conditions (30).

The similarities between this nitrogen resonance and that thought to be due to ionized nitrogen pairs suggests that this ESR spectrum may be caused by a preferentially oriented nitrogen pairs. This model would be consistent with the effects of UV-irradiation on the ESR spectrum in samples D-60 and D-61.

A SELECTED BIBLIOGRAPHY

(1) E. J. Zavoisky, "Paramagnetic Absorption in Some Salts in Perpendicular Magnetic Fields," Phys. USSR 10, 170 (1946).

(2) W. J. Leivo and R. Smoluchowski, "A Semiconducting Diamond," Phys. Rev. 98, 1532 (1955).

(3) P. A. M. Dirac, Principles of Quantum Mechanics (Oxford at the Clarendon Press, Oxford, 1959).

(4) R. Robertson, J. J. Fox and A. E. Martin, "Two Types of Diamond," Phil. Trans. Roy. Soc. (London) A232, 463 (1934).

(5) G. B. B. M. Sutherland, D. E. Blackwell and W. G. Simeral, "The Problem of the Two Types of Diamond," Nature 174, 901 (1954).

(6) C. D. Clark, R. W. Ditchburn and H. B. Dyer, "The Absorption Spectra of Natural and Irradiated Diamonds," Proc. Roy. Soc. (London) A234, 363 (1956).

(7) J. F. H. Custers, "Unusual Phosphorescence of a Diamond," Physics 18, 489 (1952).

(8) J. F. H. Custers, "Semiconductivity of Type IIb Diamonds," Nature 176, 173 (1955).

(9) J. F. H. Custers, "Type IIb Diamond," Physica 20, 183 (1954).

(10) H. J. Stein, "Determination of Energy Levels in Semiconducting Diamond By Transmission Method," (M.S. Thesis, Oklahoma State University, 1960).

(11) R. H. Wentorf, Jr., and H. P. Bovenkerk, "Preparation of a Semiconducting Diamonds," J. Chem. Phys. 36, 1987 (1962).

(12) F. A. Raal, "A Spectrographic Study of the Minor Element Content of Diamond," Am. Mineral 42, 354 (1957).

(13) J. H. E. Griffiths, J. Owen and I. M. Ward, "Magnetic Resonance in Irradiated Diamond and Quartz," Conference on Defects in Crystalline Solids (Physical Society, London, 1955) p. 81.

(14) M. C. M. O'Brien and M. H. L. Pryce, "Paramagnetic Resonance in Irradiated Diamond and Quartz," Conference on Defects in Crystalline Solids (Physical Society, London, 1955) p. 88.

(15) E. A. Faulkner and J. H. Lomer, "Electron Spin Resonance in Electron Irradiated Diamond," Phil. Mag. 7, 1995 (1962).

(16) T. Yamaguchi, "Electronic States of Single Vacancies in Diamonds," J. Phys. Soc. Japan 17, 1359 (1962).

(17) T. Yamaguchi, "Electronic States of Single Interstitial in Diamonds," J. Phys. Soc. Japan 18, 368 (1963).

(18) C. A. Coulson and M. J. Kearsley, "Color Centers in Irradiated Diamonds I," Proc. Roy. Soc. (London) A241, 433 (1957).

(19) M. Lax and E. Burstein, "Infrared Lattice Absorption in Ionic and Homopolar Crystals," Phys. Rev. 97, 39 (1955).

(20) S. D. Smith and J. R. Hardy, "Activation of Single Phonon Infrared Lattice Absorption in Neutron Irradiated Diamond," Phil. Mag. 5, 1311 (1960).

(21) F. C. Frank, "On the X-ray Diffraction Spikes of Diamond," Proc. Roy. Soc. (London) A237, 168 (1956).

(22) S. Catiche-Ellis and W. Cochran, "The X-ray Diffraction Spikes of Diamond," Acta. Cryst. 11, 245 (1958).

(23) W. Kaiser and W. L. Bond, "Nitrogen, A Major Impurity in Common Type I Diamond," Phys. Rev 115, 857 (1959).

(24) E. C. Lightowlers and P. J. Dean, "Measurement of Nitrogen Concentration in Diamond by Photon Activation Analysis and Optical Absorption," Diamond Research (1964).

(25) W. V. Smith, P. P. Sorokin, I. L. Gelles and G. J. Lasher, "Electron Spin Resonance of Nitrogen Donors in Diamond," Phys. Rev. 115, 1546 (1959).

(26) H. J. Bower and M. C. R. Symons, "Electron Spin Resonance Spectra Associated With Nitrogen in Diamond," Nature 210, 1037 (1966).

(27) R. J. Elliott, "Speculations on the Centers Formed by Nitrogen in Diamond," Proc. Phys. Soc. (London) 76, 787 (1960).

(28) T. Evans and C. Phaal, "Imperfections in Type I and Type II Diamonds," Proc. Roy. Soc. (London) A270, 538 (1962).

(29) P. F. James and T. Evans, "Diffraction Contrast From Precipitates in Type I Diamonds," Phil. Mag. 11, 113 (1965).

(30) R. J. Caveney, "The Reciprocal Lattice Spikes in Type Ia Diamonds," Phil. Mag. 18, 193 (1969).

(31) N. D. Samsonenko, "Distribution of Paramagnetic Nitrogen Centers in Some Type I Diamonds," Soviet Phys.-Solid State 6, 2460 (1965).

(32) J. H. N. Loubser and L. DuPreez, "New Lines in the Electron Spin Resonance Spectrum of Substitutional Doners in Diamond," Brit. J. Appl. Phys. 16, 457 (1965).

(33) W. V. Smith, I. L. Gelles and P. P. Sorokin, "Electron Spin Resonance of Acceptor States in Diamond," Phys. Rev. Letter 2, 39 (1959).

(34) J. A. Baldwin, Jr., "Electron Paramagnetic Resonance Investigation of the Vacancy in Diamond," Phys. Rev. Letters 10, 220 (1963).

(35) M. D. Bell and W. J. Leivo, "Electron Spin Resonance in Semiconducting Diamonds," J. Appl. Phys. 38, 337 (1967).

(36) P. E. Klingsporn, M. D. Bell, and W. J. Leivo, "Analysis of an Electron Spin Resonance Spectrum in Natural Diamonds," J. Appl. Phys. 41, 2977 (1970).

(37) J. P. King, M. D. Bell, and W. J. Leivo, "Effects of Light on the Electron Spin Resonance of Diamond," Bull. Am. Phys. Soc. 11, 834 (1966).

(38) R. Berman, Physical Properties of Diamond (Clarendon Press, Oxford, 1965).

(39) F. Bloch, "Nuclear Induction," Phys. Rev. 70, 460 (1946).

(40) J. I. Rabi, N. F. Ramsey and J. Schwinger, "Use of Rotating Coordinates in Magnetic Resonance Problems," Rev. Mod. Phys. 26, 167 (1954).

(41) C. P. Slichter, Principles of Magnetic Resonance (Harper and Row, New York, 1963).

(42) A. H. Cooke, "Paramagnetic Relaxation Effects," Rept. on Prog. in Phys. 13, 276 (1950).

(43) R. De L. Kronig, "On the Mechaniques of Paramagnetic Relaxation," Physica 6, 33 (1939).

(44) J. H. Van Vleck, "Paramagnetic Relaxation Times for Titanium and Chrome Alum," Phys. Rev. 57, 426 (1940).

(45) G. E. Pake, "Fundamentals of Nuclear Magnetic Resonance Absorption," Am. J. of Phys. 18, 438 (1950).

(46) W. Low, "Paramagnetic Resonance in Solids," Solid State Phys. Supplement 2, 1 (1960).

(47) G. E. Pake, Paramagnetic Resonance (W. A. Benjamin, New York, 1962).

(48) M. H. L. Pryce, "A Modified Perturbation Procedure for a Problem in Paramagnetism," Proc. Phys. Soc. (London) A63, 25 (1950).

(49) A. Abragam and M. H. L. Pryce, "Theory of Nuclear Hyperfine Structure of Paramagnetic Resonance Spectra in Crystals," Proc. Roy. Soc. (London) A205, 135 (1951).

(50) B. Bleaney and K. W. H. Stevens, "Paramagnetic Resonance," Repts. on Prog. in Phys. 16, 108 (1953).

(51) K. D. Bowers and J. Owen, "Paramagnetic Resonance II," Rept. on Prog. in Phys. 18, 304 (1955).

(52) G. Breit and I. I. Rabi, "Measurement of Nuclear Spin," Phys. Rev. 38, 2082 (1931).

(53) M. D. Bell, "Electron Spin Resonance in Diamond," (Ph. D. thesis, Oklahoma State University, 1964).

(54) J. P. Gordon, "Variable Coupling Reflection Cavity for Microwave Spectrometer," J. Sci. Instr. 39, 658 (1961).

(55) R. V. Pound, "Frequency Stabilization of Microwave Oscillators," Proc. of IRE 34, 1405 (1947).

(56) C. G. Montgomery, Techniques of Microwave Measurements, MIT Radiation Lab. Series, Vol. 11, (McGraw-Hill, New York, 1947).

(57) M. W. P. Stranberg, M. Tinkham, I. H. Solt, Jr., and C. F. Davis "Recording Magnetic-Resonance Spectrometer," Rev. Sci. Instr. 27, 596 (1956).

(58) J. C. Slater, Microwave Electronics, (D. Van Nostrand Co., New York, 1950).

(59) F. A. Faulkner, "Improved Circuit for an Electron Spin Resonance Spectrometer," J. Sci. Instr. 39, 135 (1962).

(60) B. Lax and K. J. Button, Microwave Ferrites and Ferrimagnetics (McGraw-Hill Co., New York, 1962).

(61) C. P. Poole, Jr., Electron Spin Resonance, (John Wiley and Sons, New York, 1967).

(62) R. Ager, T. Cole and J. Lambe, "Coupling Scheme for Microwave Cavities," Rev. Sci. Instr. 32, 658 (1961).

(63) J. W. M. DuMond and E. R. Cohen, Handbook of Physics (McGraw-Hill Co., New York, 1958), p. 7-170.

(64) A. G. Every and D. S. Schonland, "A Donor Electron Orbital for Nitrogen in Diamond," Solid State Connun. 3, 205 (1965).

(65) M. Ya. Shcherbakova, E. V. Sobolev, N. D. Sansonenko, and V. K. Aksenov, "Electron Paramagnetic Resonance of Ionized Nitrogen Pairs in Diamond," Soviet Phys.-Solid State 11, 1104 (1969).

(66) J. P. King, "Effects of Light on the Electron Spin Resonance of Diamond," (Ph. D. thesis, Oklahoma State University, 1966).

(67) F. G. Chesley, "Investigation of the Minor Elements in Diamond," Am. Mineral. 27, 20 (1942).

(68) P. E. Klingsporn, "Analysis of Unusual Electron Spin Resonance Spectra in Diamonds", (Ph. D. thesis, Oklahoma State University, 1969).

VITA

William Carl Steckelberg

Candidate for the Degree of

Doctor of Philosophy

Thesis: ANALYSIS OF THE ELECTRON SPIN RESONANCE SPECTRUM OF A PREFERENTIALLY ORIENTED DEFECT CENTER IN DIAMONDS

Major Field: Physics

Biographical:

Personal Data: Born in Henryetta, Oklahoma, January 13, 1941, the son of Carl S. and Juanita Steckelberg.

Education: Attended grade school in Henryetta, Oklahoma; graduated from Henryetta High School in 1959; attended Westminster College in Fulton, Missouri, 1959-1960; received the Bachelor of Science degree from the Carnegie Institute of Technology, with a major in physics, in 1964; completed the requirements for the Doctor of Philosophy degree in May, 1971.

Experience: Employed as a laboratory assistant in the crystallography laboratory of the University of Pittsburg, for the summers of 1962, 1963; graduate teaching assistant in undergraduate laboratories, 1965-1967, and student instructor of general physics, at Oklahoma State University, 1968-1970.

Organizations: Member of Sigma Pi Sigma.